VISUALIZATION

OF

MOLECULAR DYNAMICS

SIMULATIONS

by

Ratan Kumar V. Mandavilly

ABSTRACT

Molecular dynamics (MD) calculations generate a large amount of data, in the form of trajectories consisting of hundreds or thousands of frames of atomic coordinates and velocities. Visualization or graphical display of such trajectories is very helpful, both as a visual check of the validity of the dynamics calculation, and as a means of focusing on any interesting behavior exhibited by the system as it evolves. Thus, visualization is both an MD validation tool and an MD analysis tool.

This work demonstrates the advantages of incorporating visualization to MD simulations. Shear viscosity for some of the Lennard-Jones fluid systems is determined using non-equilibrium MD simulations. Simulation results are validated using visualization. Screen shots of the simulations are available. The results are also compared to the available literature and experimental data.

Over the years, MD simulations have been performed to study the behavior of fluids at the sub-continuum level, for which experiments are unable to provide the requisite answers. Some of the sub-continuum fluid problems that have been studied by molecular simulations are discussed. Study of coalescence of liquids at the liquid-liquid interface is one of those sub-continuum fluid problems. To get an insight into the small-scale dynamics of the coalescence process, molecular dynamics simulations of

coalescence in systems of about 864 Lennard-Jones particles have been performed in this work. Analysis of the simulations results using visualization clearly show the events involved in the coalescence process.

ACKNOWLEDGMENTS

I would like to acknowledge, first and foremost, the guidance and support provided by my advisor, Prof James. F. Ely. In addition, the wealth of experience and insights that he provided in solving the various problems encountered during this work helped shape this final product.

I wish to thank the department system administrator Steve Toleque for maintaining and upgrading the computer network from time to time.

Thanks to my officemate Haizhong for helping me with some of the problems I faced during the course of this project. Thanks to my friends-Ragu, Sanga, Raghav, Cas, Prakash, Ananth, Nikhil, Kini, Phani and Premal for helping me through times of trouble.

TABLE OF CONTENTS

LIST OF FIGURES

LIST OF TABLES

Chapter 1

INTRODUCTION

Molecular dynamics (MD) simulation provides the methodology for detailed microscopic modeling on the molecular scale (Rapaport, 1995). After all, the nature of matter is to be found in the structure and motion of its constituent building blocks, and the dynamics is contained in the solution to the *N*-body problem. Given that the classical *N*-body problem lacks a general analytical solution, the only path open is the numerical one. Scientists engaged in studying matter at this level require computational tools to allow them to follow the movement of individual molecules and it is this need that the molecular dynamics approach aims to fulfill.

Over the years, MD simulations have been used to study a wide range of problems falling under various categories. Some of the categories and the interesting problems in each of the categories are listed below:

- Fundamental studies: kinetic theory, diffusion, transport properties, tests of models and potential functions.
- Phase transitions: first- and second- order, phase coexistence.

- Collective behavior: decay of space- and time- correlation functions, spectroscopic responses.
- Complex fluids: structure and dynamics of glasses, ionic fluids, fluid interfaces and liquid crystals.
- Polymers: chains, rings and branched molecules, membranes, crystallite formation.
- Solids: defect formation, grain boundaries, elastic properties.
- Fluid dynamics: laminar flow, boundary layers, rheology of non-Newtonian fluids, subcontinuum fluid problems and the list goes on.

Generally speaking, MD can explore any phenomena that occur on length and time scales that are encompassed by the computation. However, owing to the purely classical nature of MD and the hardware-imposed computational limitations, MD does not benefit some of the other application areas.

Computations using MD are no longer merely number crunching. Along with ready access to high-performance computing comes the ability to actually observe or visualize the system being simulated (Rapaport, 1997). In particular, graphics can be used to visualize the system being simulated. The MD practitioner need no longer be content with graphs of P plotted as a function of T, or some correlation as a function of time, but is now able to observe a system as it evolves, letting the eye capture some of the more subtle cooperative effects as the molecules reorganize. If we consider simulations as computer experiments, this visual approach can be considered as the computational analog of the optical microscope. Visualization itself takes many forms. Representing the results of discrete particle simulations offers a choice between direct observation of the particles themselves, or a display, typically involving scalar or vector fields, of suitably averaged quantities such as velocity, vorticity, temperature, etc. Data may be represented by means of arrow, contour, and surface plots as well as in less conventional, but visually rich forms, including extensive use of color and animation.

Using visualization in MD simulations has two main advantages. It serves as a (a) validation tool and (b) analysis tool for the results obtained from the simulations. The main objective of this work is to demonstrate these above-mentioned advantages of incorporating visualization in molecular dynamics simulations. Two case studies are chosen for this purpose.

In the first case study MD simulations were performed to determine the viscosity of the following systems:

1. Pure single site Lennard-Jones (LJ) fluids.
2. Binary mixtures of single site LJ fluids.
3. Structured molecules made up of multiple LJ sites.

Viscosity can be determined either by using equilibrium molecular dynamics (EMD) or by non-equilibrium molecular dynamics (NEMD) technique. In this work the latter technique was chosen to perform the viscosity calculations for all the three systems mentioned above. Further, equilibrium molecular dynamic simulations of dilute solutions of benzene in supercritical CO_2 were performed.

In the second case study molecular dynamic simulations were performed to study one of the subcontinuum fluid problems: the coalescence process at a liquid-liquid interface.

In both the case studies, visualization is incorporated in the simulation code using OpenGL libraries. The code for simulations is itself written in C++. OpenGL is a platform independent application program interface to the graphics hardware (Neider, Davis et al., 1999). The graphics routines can be directly called from Fortran or C code used for programming the simulations.

This report is organized in the following manner. The rest of this chapter discusses the molecular dynamics technique (Haile, 1997) in detail and gives the mathematical background for the equations used to model the system being simulated. Chapter 2 presents the theoretical background for the shear viscosity calculations using non-equilibrium molecular dynamics. Results obtained for shear viscosity of pure LJ fluids, LJ binary mixtures as well as structured molecules like carbon dioxide are reported and comparisons are made with available literature data. Screen shots of the simulations are also shown. Chapter 3 presents a review of some of the very interesting subcontinuum fluid problems that are being studied by molecular dynamics simulations for which experiments are unable to provide the requisite answers. Chapter 4 presents the second case study, which is one of the subcontinuum fluid problems (coalescence process) described in chapter 3. The first part of the chapter 4 discusses the coalescence phenomenon at liquid-liquid interface and some of the hydrodynamic models used to understand the observations. Further, the need for studying coalescence process using MD is explained. The later part of the chapter 4 presents the simulation studies for the coalescence process. It shows some of the results obtained from the simulations of coalescence systems. Screen shots showing the steps involved in the coalescence process are available. It also presents a comparison between the experiments and simulations. Conclusions and scope for future work are discussed in chapter 5.

1.1 Overview of molecular dynamics

Molecular dynamics simulation is a technique to compute the equilibrium and transport properties of a classical many-body system. The basic steps involved in a typical MD simulation are shown in Figure 1.1. In an equilibrium molecular dynamics, we start simulations of a particular system with hundreds to thousands of molecules in an initial configuration. Then the macroscopic state we want to achieve is specified by a combination of temperature, density and/or pressure. Each molecule is assigned a random velocity corresponding to the overall kinetic energy specified by the temperature conditions. The system is then allowed to reach this state at which time we say the system has equilibrated.

The motion of the molecules is determined by equations of motion over the entire period of simulation. Starting from the initial configuration, the forces acting on each molecule are determined from an assumed interaction potential model between the

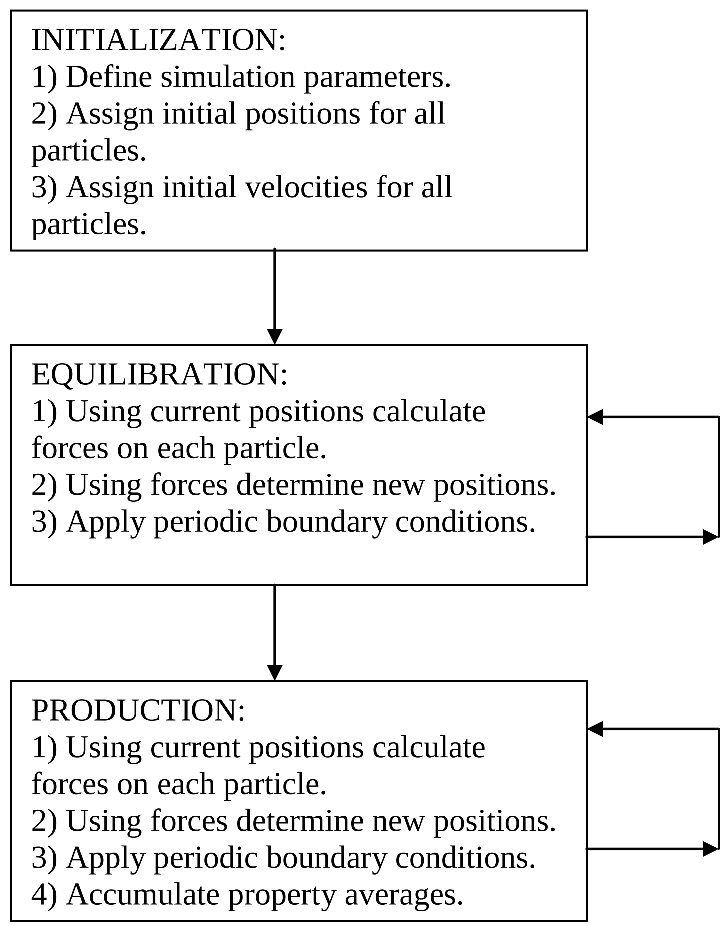

Figure 1.1: Flow chart for the basic steps involved in a MD simulation

molecules. Common examples include the Lennard-Jones potential, square well potential, exponential-six, etc. Once the forces on each molecule are determined, we can use Newton's laws of motion or the equivalent Hamiltonian equations of motion to determine the new position of each molecule after a small time step. The equations of motion for all the molecules have to be solved simultaneously to get positions and velocities of molecules as a function of time. Owing to the lack of an analytical solution for the same, we resort to a numerical technique called the finite difference method, which assumes time elapses in a stepwise manner. Based on the configuration at an earlier time step one can calculate the configuration at the next time step. The length of time step is hard coded in the simulations and the value is determined depending on various factors. The equations and variables of motion are non-dimensionalized appropriately as summarized in Table 1.1.

1.1.1 Equations of motion

In the Newtonian dynamics the motion and the applied force are explicitly related through Newton's second law,

$$\mathbf{F}_i = m\ddot{\mathbf{r}}_i \tag{1.1}$$

The equivalent Hamiltonian equations of motion are given by

$$\begin{aligned} \dot{\mathbf{r}}_i &= \frac{\mathbf{p}_i}{m} \\ \dot{\mathbf{p}}_i &= \mathbf{F}_i \end{aligned} \tag{1.2}$$

Table 1.1: System of units used in soft-sphere molecular dynamics program

Variable	Reduced Unit
Fundamental Quantities	
Mass	m (mass of one atom)
Length	σ (LJ diameter of one atom)
Energy	ε (LJ interaction parameter)
Time	$\sigma\sqrt{m/\varepsilon}$
Derived Quantities	
Temperature	$T^* = kT/\varepsilon$
Density	$\rho^* = N\sigma^3/V$
Force	$F^* = F\sigma/\varepsilon$
Velocity	$v^* = v\sqrt{m/\varepsilon}$
Pressure	$P^* = P\sigma^3/\varepsilon$
Viscosity	$\eta^* = \eta\sigma^2/\sqrt{m\varepsilon}$
Strain Rate	$\gamma^* = \gamma\sigma\sqrt{m/\varepsilon}$

where $\mathbf{r}_i$ and $\mathbf{p}_i$ are the position and momentum vectors of the i^{th} particle and the dots above the vectors represent the time derivatives.

In the equation below $\mathbf{F}_{ij}$ is the force exerted by particle *j* on the i^{th} particle and is given by:

$$\mathbf{F}_{ij} = -\frac{\partial U(\mathbf{r}^N)}{\partial \mathbf{r}_{ij}} \tag{1.3}$$

and the net force $\mathbf{F}_i$ acting on particle *i* is the sum of the forces from all particles. The notation $\mathbf{r}^N$ represents the set of position vectors for all the *N* particles in the system $\mathbf{r}^N = \{\mathbf{r}_1, \mathbf{r}_2 \ldots, \mathbf{r}_N\}$ and U is the potential of the entire configuration. It is evaluated by summing over all the pair-wise potentials by neglecting higher order interactions.

$$U = \sum_i \sum_{j>i} u(r_{ij}) \tag{1.4}$$

The pair-wise potential is given by the model we choose. A commonly used intermolecular potential is the Lennard-Jones (LJ) potential.

$$u(r_{ij}) = 4\varepsilon\left[\left(\frac{\sigma}{r_{ij}}\right)^{12} - \left(\frac{\sigma}{r_{ij}}\right)^{6}\right] \tag{1.5}$$

where σ and ε are the LJ distance and energy parameters (Figure 1.2) and r_{ij} is the scalar distance between the particles i and j. All the equations are first non-dimensionalized using the definitions in Table 1.1.

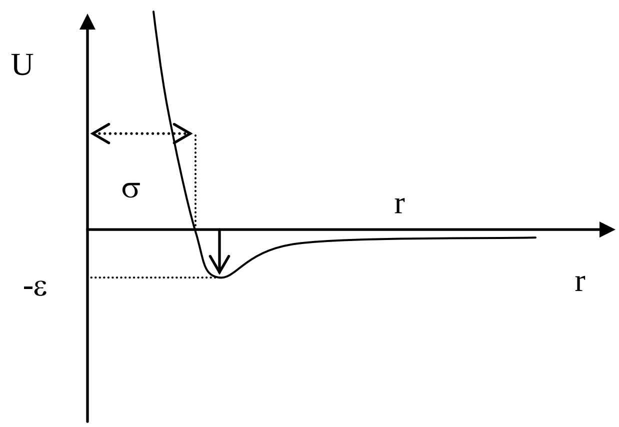

Figure 1.2: Lennard-Jones (12-6) pair potential

Once the forces on each particle are evaluated one can solve the equations of motion given by Eqn (1.2) and Eqn (1.3) by finite-difference methods. Various techniques used to solve these include: Verlet's leap frog method, Runge-Kutta, Gear predictor-correctors, etc. In this work fourth-order Gear predictor-corrector method (Allen and Tildesley, 1989) is used and is explained in greater detail below.

Predictor-corrector methods are composed of three steps: prediction, evaluation and correction. In particular, from the current position $\mathbf{r}(t)$ and momentum $\mathbf{p}(t)$ the steps are as follows:

1. Based on the current position $\mathbf{r}(t)$ and momentum $\mathbf{p}(t)$, predict the position $\mathbf{r}(t+\Delta t)$ and momentum $\mathbf{p}(t+\Delta t)$ and the values of their higher order derivatives at the end of the next step.
2. Evaluate the forces at $t+\Delta t$ using the above predicted positions.
3. Use the force and predicted momentum to determine the error made in the estimation of second derivative of position and first derivative of momentum. Further, based on these errors all other derivatives of position and momentum are corrected.

As a specific example of a predictor-corrector algorithm, consider the Taylor series expansion for the position of a given particle at time $t+\Delta t$:

$$\mathbf{r}(t+\Delta t) = \mathbf{r}(t) + \Delta t \frac{\partial \mathbf{r}}{\partial t} + \frac{\Delta t^2}{2!}\frac{\partial^2 \mathbf{r}}{\partial t^2} + \frac{\Delta t^3}{3!}\frac{\partial^3 \mathbf{r}}{\partial t^3} + \cdots \tag{1.6}$$

Using the notation

$$\begin{aligned}
\mathbf{x0}(t) &\equiv \mathbf{r}(t) \\
\mathbf{x1}(t) &\equiv \Delta t \frac{\partial \mathbf{r}}{\partial t} \\
\mathbf{x2}(t) &\equiv \frac{\Delta t^2}{2!}\frac{\partial^2 \mathbf{r}}{\partial t^2} \\
\mathbf{x3}(t) &\equiv \frac{\Delta t^3}{3!}\frac{\partial^3 \mathbf{r}}{\partial t^3}
\end{aligned}$$

Then we can write the predictions for $\mathbf{x0}(t+\Delta t)$ through $\mathbf{x3}(t+\Delta t)$:

$$\begin{aligned}
\mathbf{x0}(t+\Delta t) &= \mathbf{x0}(t) + \mathbf{x1}(t) + \mathbf{x2}(t) + \mathbf{x3}(t) \\
\mathbf{x1}(t+\Delta t) &= \phantom{\mathbf{x0}(t)} + \mathbf{x1}(t) + 2\mathbf{x2}(t) + 3\mathbf{x3}(t) \\
\mathbf{x2}(t+\Delta t) &= \phantom{\mathbf{x0}(t) + \mathbf{x1}(t)} + \mathbf{x2}(t) + 3\mathbf{x3}(t) \\
\mathbf{x3}(t+\Delta t) &= \phantom{\mathbf{x0}(t) + \mathbf{x1}(t) + \mathbf{x2}(t)} + \mathbf{x3}(t)
\end{aligned} \tag{1.7}$$

Now that we have $\mathbf{x0}(t+\Delta t)$, we can compute the forces at the predicted position, and thus compute the corrected value for acceleration. We denote the difference between $\mathbf{x2}^{corrected}$ and $\mathbf{x2}^{predicted}$ by $\Delta\mathbf{x2}$:

$$\Delta\mathbf{x2} \equiv \mathbf{x2}^{corrected} - \mathbf{x2}^{predicted}$$

We now estimate the "corrected" values for x through $x3$, as follows:

$$\mathbf{xn}^{corrected} = \mathbf{xn}^{predicted} + C_n \Delta\mathbf{xn} \tag{1.8}$$

where the C_n are constants for a given order of the algorithm. As indicated the values for C_n are such that they yield an optimal compromise between the accuracy and stability of the algorithm. For instance, for a fourth-order predictor-corrector algorithm the values for C_n are given by $C_0 = \frac{19}{120}; C_1 = \frac{3}{4}; C_2 = 1; C_3 = \frac{1}{2}; C_4 = \frac{1}{12}$.

1.1.2 Property calculations

For a system of N particles, the phase-space trajectory is represented by the set of generalized coordinates

$$\left\{ \left[\mathbf{r}^N(k\Delta t), \mathbf{p}^N(k\Delta t) \right], k = 1, \ldots\ldots, M \right\}$$

where $\mathbf{r}^N$ is the set of N position vectors and $\mathbf{p}^N$ is the set of N momentum vectors. The trajectory is obtained from a simulation performed over M discrete times using the time-step Δt. From this trajectory the time average $\langle A \rangle$ of some function of the trajectory can be estimated by the sum:

$$\langle A \rangle = \frac{1}{M}\sum_{k=1}^{M} A\left[\mathbf{r}^N(k\Delta t), \mathbf{p}^N(k\Delta t)\right] \tag{1.9}$$

The above finite interval average is an approximation to the infinite time average

$$\langle A \rangle = \lim_{t\to\infty}\frac{1}{t}\int_{t_o}^{t_o+t} A(\mathbf{r}^N, \mathbf{p}^N)d\tau$$

Expressions for some of the equilibrium properties are given below. Temperature is calculated from the expression for average kinetic energy:

$$\langle E_k \rangle = \frac{3}{2}Nk_BT = \frac{1}{2mM}\sum_{k=1}^{M}\sum_{i=1}^{N}\mathbf{p}_i(k\Delta t)\cdot\mathbf{p}_i(k\Delta t) \tag{1.10}$$

Configurational energy is the average of the pair-wise potential function $u(r)$,

$$U_c = \frac{1}{M}\sum_{k=1}^{M}\sum_{i}\sum_{j>i}u[\mathbf{r}_{ij}(k\Delta t)] \tag{1.11}$$

Pressure P is related to molecular quantities through the virial of the force:

$$\frac{P}{\rho kT} = 1 - \frac{1}{3NkT}\left\langle \sum_{i}\sum_{j>i} r_{ij}\frac{du(r_{ij})}{dr_{ij}} \right\rangle \tag{1.12}$$

The first term on the right hand side is the ideal-gas contribution, and the second term accounts for intermolecular forces, assuming a pair-wise additive potential $u(r)$. The intermolecular potential is either truncated or truncated and shifted at a cut-off radius, r_c, and in the case of truncated interactions, the pressure P and internal energy U are corrected by adding the tail contributions given by the expressions below:

$$
\begin{aligned}
P^{tail} &\approx -\frac{16\pi\rho}{3T(r_c)^3} \\
U^{tail} &\approx -\frac{8\pi\rho}{3(r_c)^3}
\end{aligned}
\tag{1.13}
$$

1.2 Visualization and interactivity

As mentioned earlier in this chapter, visualization is an important MD validation and analysis tool. Interactivity, on the other hand provides a better user interface or environment to run the simulations. Visualization of the simulations can take many forms. The most immediate form is the viewing of the individual particles as they interact with one another. For example, it may be a graphical picture showing the particles in the system as small spheres or discs. The graphics can be either 2-D or 3-D. The trajectory of the particles can be directly viewed by looking at their positions. The graphics screen is required to be updated for every few time steps since the positions of the particles keep changing every time step during the simulations. In showing the trajectories of particles there are no time averages involved. In contrast to this, one may be interested in visualizing the density or velocity fields where we need to obtain some time averages before displaying them using graphics. Interactivity provides a way for the user to control the parameters of the simulation and the computation process itself and also to control the graphic output of the computation.

Typically, while the computations can be programmed in some standardized system independent language, such as C, the programming required to provide the graphics and interactivity is very much system dependent. There has been a lot of software development over the past few years, which provide good graphics interfaces. For the Unix-based systems the availability of the X-windows environment for graphics and Motif for interface development helped programmers to incorporate visualization and interactivity in their programs. For more advanced three-dimensional graphics, OpenGL software is now available on most platforms. Even though the underlying logic of the software needed for visualization and user interfacing remains the same, irrespective of the platform, the actual implementation on a machine such as the Macintosh is very different from X/Motif.

Chemists today are presented with a wide choice of commercial and academic visualization software packages. Many of these software packages have overlapping capabilities, and the choice of one over the other may just be a matter of user preference. However, strong factors in the choice of a particular program may involve compatibility with the format of a user's data set, output options. Using OpenGL, with little effort we can add visualization code into the simulations program.

We must always worry about the reliability of any simulation. Typically, one has to validate the results of simulation. The issue of validity is analogous to the issue of accuracy in laboratory experiments. By incorporating visualization we can right away detect if the system is demonstrating unexpected dynamics. For example if we are simulating a system of molecules with some particular constraints on the bond lengths, typically these constraints are incorporated in the equations of motion. In such cases, it is possible that our simulations may give what we think are “acceptable” values for the properties we are interested in, but on the other hand, in reality, the constraints may not be followed well. This can be readily validated by visualization. We can actually see the molecules elongating or contracting if the bond length constraints are not met. This kind of validation is important especially if we do not have experimental data or an analytic theory results to compare with our simulation results. An example is in the case of novel systems that have not been studied previously. Some more advantages of having visualization are:

1. It helps us to get an idea how well the system has equilibrated so that we can start accumulating time averages.
2. It helps us to know if the periodic boundary conditions are being applied well. It helps us to detect any strange behavior at the walls or the boundaries.
3. It can be used in demonstrating interesting phenomenon at molecular level that cannot be observed in the laboratory.

The objective of this study is to add visualization capabilities to some of our simulations code and demonstrate its advantages.

Chapter 2

MOLECULAR DYNAMICS SIMULATIONS FOR SHEAR VISCOSITY

This chapter presents the results of viscosity calculations done using non-equilibrium molecular dynamics for both pure Lennard-Jones fluids and also for binary mixtures of Lennard-Jones fluids. The fluid systems studied in this part of our work for viscosity calculations are (a) liquid argon, (b) liquid krypton, (c) a mixture of liquid argon and liquid krypton at varied compositions (d) and pure carbon dioxide. For the first three systems, the molecules are modeled as single site LJ particles contrary to the pure carbon dioxide, which is considered as a structured molecule and modeled as a combination of three LJ site particles. The results obtained in each case are compared to the experimental and literature values. Screen shots of the simulation box and velocity profiles that develop in the systems under shear are also presented. In the final section of the chapter, results obtained from the equilibrium simulations of dilute solutions of benzene in carbon dioxide are presented.

Prior to presenting simulation results, the physical meaning of viscosity and the methodology followed to determine its value from molecular dynamics simulations are discussed briefly.

2.1 Newton's law of viscosity

Consider a fluid contained between two large parallel plates of area A, which are separated by a very small distance Y. We imagine that the system is initially at rest but at time $t = 0$ the upper plate is set in motion in the x-direction at a constant velocity V. As the time proceeds, the fluid gains momentum, and finally a steady-state profile shown in Figure 2.1 is established. This kind of flow is also termed as Couette flow.

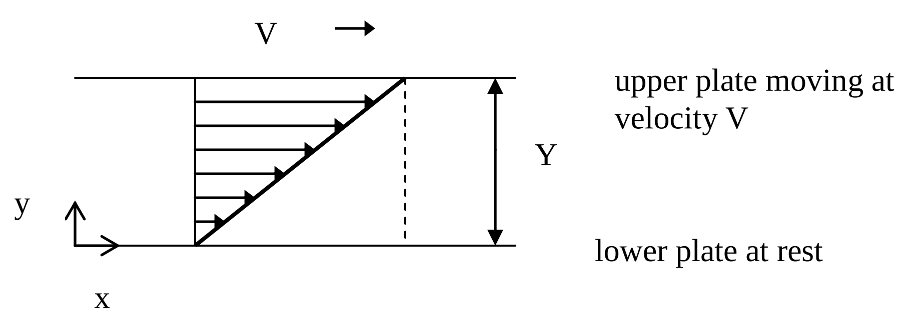

Figure 2.1: Velocity profile for fluid contained between two plates and subjected to Couette flow.

When this final state of steady motion is attained, a constant force F is required to maintain the motion of upper plate. This force is expressed as follows (provided the flow is laminar):

$$\frac{F}{A} = \eta \frac{V}{Y} \tag{2.1}$$

i.e. the force per unit area is proportional to the velocity decrease in distance Y; the constant of proportionality η is called the viscosity of the fluid. For this case, the pressure tensor $\mathbf{P}$ is given by:

$$\mathbf{P} = p\mathbf{U} + \tau \tag{2.2}$$

where $\mathbf{U}$ is the unit tensor, p is the static pressure and τ is the shear stress tensor, which represents the pressure developed due to shear forces. Eqn (2.1) in a more general form is written as:

$$\tau_{yx} = -\eta \left(\frac{\partial v_x}{\partial y} \right) = -\eta \gamma \tag{2.3}$$

where τ_{yx} is the force exerted per unit area in the x-direction on a fluid surface element perpendicular to the y-direction and η is expressed as a function of shear rate

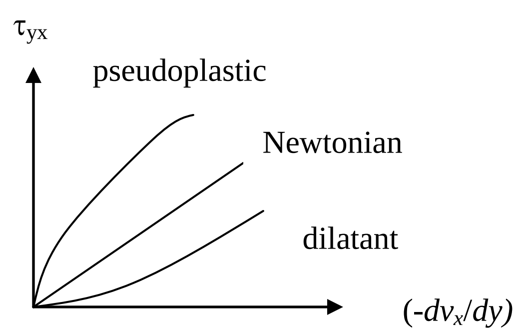

Figure 2.2: Constitutive relationships for different fluids

$\left(-dv_x/dy\right)$ or τ_{yx}. If η is independent of shear rate, the behavior is Newtonian, with $\eta = \mu$. The fluids for which η decreases with increase in shear rate are termed as pseudo plastic or shear thinning fluids. On the other hand, the fluids for which η increases with increase in shear rate are termed as dilatant or shear thickening fluids (see Figure 2.2).

2.2 Shear viscosity calculations: methodology

Because of the fundamental relations between the linear non-equilibrium response and time-dependent equilibrium fluctuations, we have two ways of calculating transport coefficients. We can perform an equilibrium simulation and calculate the appropriate equilibrium time correlation functions that give the transport coefficients. The principal advantage of this method is that all possible transport coefficients can, in principle, be calculated from a single molecular dynamics run. This approach has, however, proved to be (a) very expensive in computer time with poor signal-to-noise ratios and (b) giving results that often depend strongly and non-monotonically upon the size of the system being simulated.

The other approach of determining transport properties is by non-equilibrium molecular dynamics (NEMD). This approach eliminates the above-mentioned shortcomings of equilibrium simulations. It also has the added advantage that it can, in principle, be used to calculate nonlinear as well as the linear transport coefficients. NEMD methods rely on measuring the response of a system to perturbing field and relating the linear response to a transport coefficient. The microscopic system is simulated at a steady state away from equilibrium and the transport coefficient calculated from the ratio of current to the applied field. In the case of viscosity, the applied field is a boundary driven planar Couette flow field characterized by strain rate $\gamma = du_x / dy$ (where u_x is the velocity of the fluid in *x*-direction) and the response is the off-diagonal element of the pressure tensor, P_{xy}. The constant temperature version of the linear response theory for this problem provides an expression for η based on the pressure tensor.

$$\eta = -\lim_{\gamma \to 0} \lim_{t \to \infty} \left\langle P_{xy} \right\rangle / \gamma \tag{2.4}$$

In this work, non-equilibrium MD simulations were performed using a NVT algorithm developed by Edberg *et al*. (1986), a molecular version of the isothermal shear algorithm known as SLLOD (Evans and Morriss, 1984). Non-Newtonian SLLOD equations of motion inherently include the constraint forces that are derived following the prescription of Gauss's principle of least constraints instead of solving Newtonian equations of motion subject to constraints.

The code written as a part of this work is based on the equilibrium molecular dynamics program for Lennard-Jones fluid developed by Haile (1997). Some of the subroutines were added and others modified to make it a non-equilibrium molecular dynamics program by incorporating the above-mentioned SLLOD algorithm. In order to perform this change, the Newtonian equations of motion used in Haile's program are written in a more generalized form as given by the Hamiltonian equations of motion.

Hamiltonian equations of motion differ from Newton's equations of motion as they can be used for any coordinate system and are symmetric with respect to particle coordinates $(\mathbf{q}_i)$ and their conjugate momentum ($\mathbf{p}_i$). They are given by:

$$\dot{\mathbf{q}}_i = \frac{\partial H}{\partial \mathbf{p}_i} = \frac{\mathbf{p}_i}{m}$$

$$\dot{\mathbf{p}}_i = -\frac{\partial H}{\partial \mathbf{q}_i} = \mathbf{F}_i \tag{2.5}$$

Where H is the Hamiltonian function of the system that represents total energy of the system. The total energy is constant for microcanonical (NVE) ensemble.

$$H = E = E_k + U \tag{2.6}$$

E_k and U are the kinetic and configurational internal energy in Eqn (2.6). Computing center of mass trajectories using Hamiltonian equations of motion, then involves solving a set of 6N first order differential equations instead of the 3N second order Newtonian equations of motion. To determine viscosity in simulations, the following changes are made to Hamiltonian equations of motion, given by Eqn (2.5) and Eqn (2.6). Firstly, homogeneous shear was introduced to generate the Couette flow. Secondly, equations were modified to be isokinetic (NVT). The resulting equations are known as SLLOD equations of motion and are given below:

$$\dot{\mathbf{q}}_i = \frac{\mathbf{p}_i}{m} + \mathbf{i}\gamma y_i$$
$$\dot{\mathbf{p}}_i = \mathbf{F}_i - \mathbf{i}\gamma p_{iy} - \lambda \mathbf{p}_i \tag{2.7}$$

where $\mathbf{i}$ is the unit vector in the *x*-direction, γ is the applied shear rate and λ is the thermostatting multiplier given by:

$$\lambda = \frac{\sum_{i=1}^{N} [\mathbf{p}_i \cdot \mathbf{F}_i - \gamma p_{ix} p_{iy}]}{\sum_{i=1}^{N} \mathbf{p}_i \cdot \mathbf{p}_i} \tag{2.8}$$

These equations are combined with the Lees-Edwards “sliding brick” boundary conditions (Lees and Edwards, 1972) to complete the SLLOD algorithm. Background for the Lees-Edwards boundary conditions is described below.

Consider a simulation cube of length L subjected to Couette flow, located so that the streaming velocity (imposed bulk velocity) at the origin is zero (i.e. the cube $0 < \{x, y, z\} < L$). The laboratory velocity of particle i is then the sum of two parts; a peculiar or thermal velocity $\mathbf{c}_i$ and a streaming velocity $\mathbf{u}(\mathbf{r}_i) = \mathbf{i}\gamma y$ given by

$$\dot{\mathbf{r}}_i = \mathbf{c}_i + \mathbf{u}(\mathbf{r}_i) \tag{2.9}$$

Imagine that at $t = 0$ we have the usual periodic replication of the simulation cube where the boundary condition is

$$\mathbf{r}_i = (\mathbf{r}_i)_{\mathrm{mod}\, L} \tag{2.10}$$

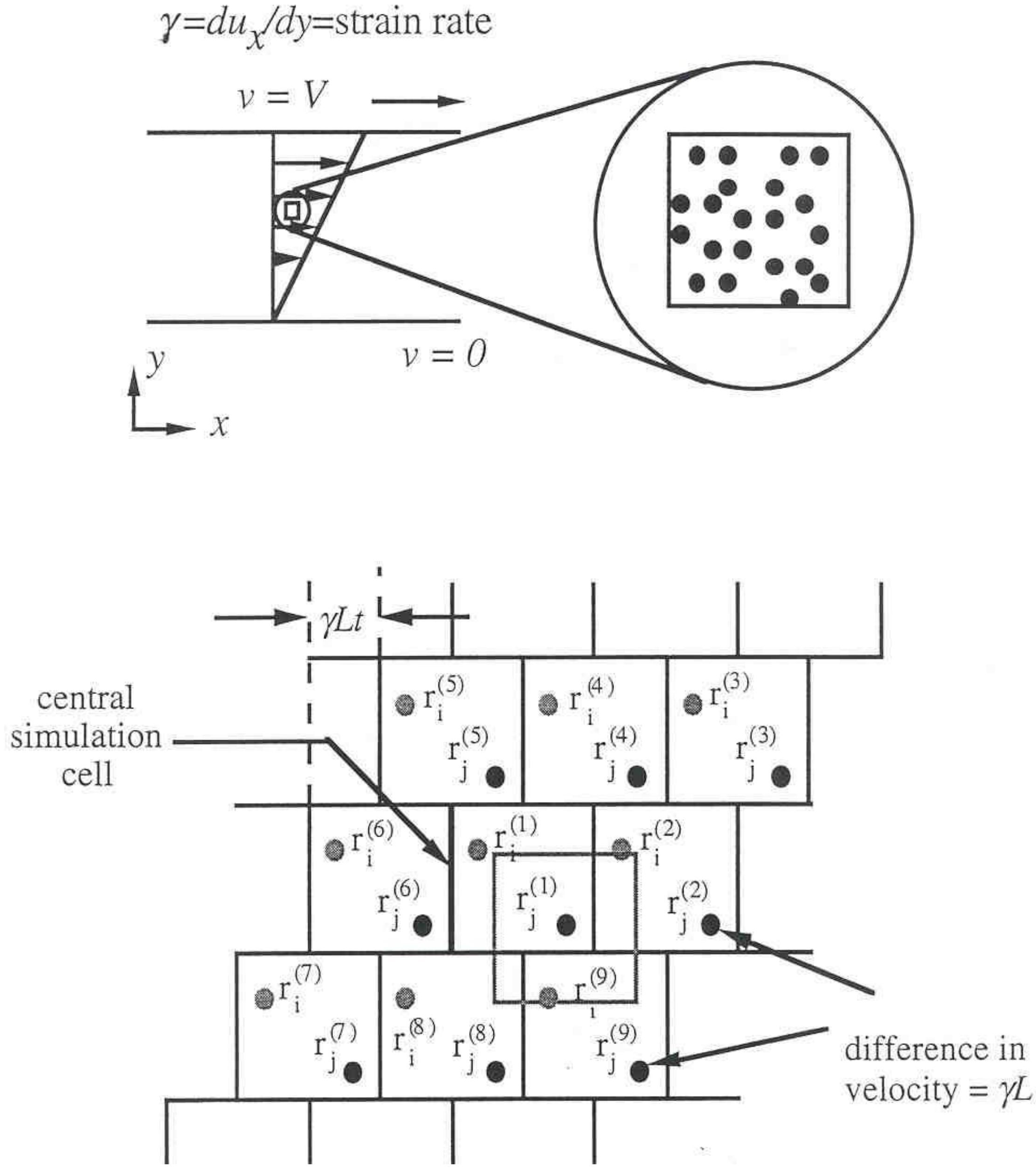

Figure 2.3: Lees-Edwards boundary conditions (Allen and Tildesley, 1989)

(this is a vector equation representing three equations in *x*, *y*, and *z* directions respectively). In *x*-direction the boundary condition is

$$x_i = (x_i)_{\mathrm{mod}\,L}$$

$$\text{if } x_i > L,\ x_i = x_i - L\ int(\frac{x_i}{L})$$

$$\text{if } x_i < 0,\ x_i = (x_i + L) - L\ int(\frac{x_i}{L})$$

Similar expressions can be written for the other two directions. As the streaming velocity is a function of y only, we need to consider explicitly boundary crossings in the y direction. At $t = 0$, $\mathbf{r}_i$ has two images $\mathbf{r}_i'$ and $\mathbf{r}_i''$ and are located at positions $\mathbf{r}_i + \mathbf{j}L$, and $\mathbf{r}_i - \mathbf{j}L$ respectively. After certain time t, we can show that:

$$\begin{aligned} \mathbf{r}_i'(t) &= \mathbf{r}_i(t) + \mathbf{j}L + \mathbf{i}\gamma Lt \\ \mathbf{r}_i''(t) &= \mathbf{r}_i(t) - \mathbf{j}L - \mathbf{i}\gamma Lt \end{aligned} \tag{2.11}$$

If $\mathbf{r}_i(t)$ moves out of the bottom of simulation cube, it is replaced by the image particle $\mathbf{r}_i'(t)$:

$$\mathbf{r}_i^{new} = (\mathbf{r}_i')_{\mathrm{mod}\,L} = (\mathbf{r}_i + \mathbf{i}\gamma Lt)_{\mathrm{mod}\,L} \tag{2.12}$$

and if $\mathbf{r}_i(t)$ moves out of the top of the simulation cube, it is replaced by the image particle at $\mathbf{r}_i''(t)$

$$\mathbf{r}_i^{new} = (\mathbf{r}_i'')_{\mathrm{mod}\,L} = (\mathbf{r}_i - \mathbf{i}\gamma Lt)_{\mathrm{mod}\,L} \tag{2.13}$$

The change in the velocity of a particle is given by the time derivatives of Eqn (2.12) and Eqn (2.13). These rules for imaging particles and their velocities are shown schematically in Figure 2.3.

The pressure tensor is calculated from the virial theorem:

$$\mathbf{P} = \frac{1}{V}\left\langle \sum_{i=1}^{N} \frac{\mathbf{p}_i \mathbf{p}_i}{m} - \frac{1}{2}\sum_{i,j}^{N} \mathbf{r}_{ij}\mathbf{F}_{ij} \right\rangle \tag{2.14}$$

and the xy components of the pressure tensor is used to calculate shear dependent viscosity from Newton’s law of viscosity

$$\eta(\gamma) = -\frac{1}{\gamma}\left\langle \frac{1}{2}P_{yx} + \frac{1}{2}P_{xy} \right\rangle \tag{2.15}$$

2.3 Velocity profile

The usual microscopic definition of temperature in terms of mean square velocity assumes that there is no overall motion; any local flow must be subtracted from the velocities before using them to evaluate temperature. However, knowing the bulk flow to an accuracy suitable for use in the equations of motion implies that the problem has already been solved; this circularity can be removed by assuming the nature of the flow, and only later checking to see whether consistent results are obtained. A less reliable alternative is to evaluate local flow by means of coarse-grained averaging, and then use the results in the equations of motion. Such an approach is unstable to any fluctuations in the flow because these variations are interpreted by the equations of motion as temperature fluctuations that must be suppressed.

In this study we assume that the MD flow obeys the linear velocity profile known from the exact solution of the continuum problem. At low shear rates and low Reynolds numbers ($Re = \rho m \gamma L^2 / \eta$) the Lees-Edwards shearing periodic boundary conditions do indeed lead to a planar velocity profile. At high Reynolds number the linear velocity profile is not stable and one needs a thermostat, which makes no assumptions whatever about the form of streaming velocity profile (Evans and Morriss, 1990).

2.4 Simulations for single site LJ molecules

Non-equilibrium MD simulations were carried out for pure argon, pure krypton and binary mixtures of both at varied compositions. Shear viscosity calculations were made using the methodology explained in section 2.2. The molecules of argon and krypton were modeled as single site LJ molecules.

2.4.1 Simulations details

The Lennard-Jones interaction parameters are given below (Table 2.1):

Table 2.1: LJ interaction parameters for argon and krypton

Interaction	σ(A^o)	ε/k_B (K)
Ar/Ar	3.405	119.8
Kr/Kr	3.633	167.0
Ar/Kr	3.519	141.4

The LJ parameters were derived on the basis of liquid state thermodynamic properties. The cross interaction parameters between Ar and Kr were calculated from the simple Lorentz-Berthelot rules.

$$\varepsilon_{ij} = (\varepsilon_i \varepsilon_j)^{1/2}$$
$$\sigma_{ij} = \frac{\sigma_i + \sigma_j}{2} \tag{2.16}$$

In the mixture simulations, the mass ratio of the atoms was taken as the corresponding molecular weight ratio of krypton and argon.

All simulations reported in this section were performed using 108-864 molecules initially in a FCC lattice and equilibrated for at least 200,000 time steps. The intermolecular potentials are subjected to a spherical cutoff radius of 2.5 times the diameter of the respective atomic pair. All the parameters used are non-dimensionalized based on the smaller atom, which in this case is argon. The code for the simulations was written in C++ (available in the accompanying CD).

2.4.2 Simulations results and discussion

Shear viscosity versus strain rate plots for pure argon and pure krypton are shown in Figure 2.4 and Figure 2.5 respectively. The simulations were carried for the reduced strain rates in the range 0.04 - 1.0. Newtonian viscosities are obtained by extrapolating the plots to zero strain rate. A comparison was done with the actual experimental viscosity values as shown in the Table 2.2. The simulation predictions are higher than the experimental values for both argon and krypton (an overestimate of 19% in the case of argon and 23% in the case of krypton). Thus, the LJ potentials can be regarded as more attractive; greater attraction would result in higher viscosities. From the

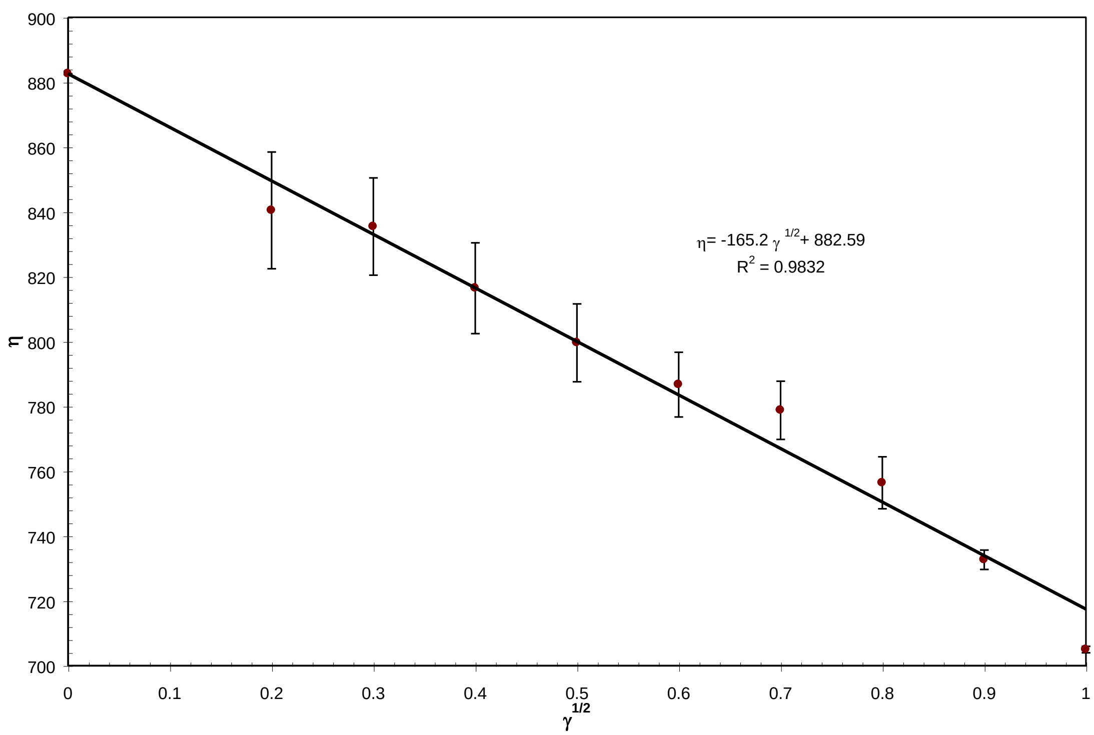

Figure 2.4: Shear viscosities (in units of 10^{-7} N s/m^2) for argon as a function of square root of strain rate (in units of ps$^{-1/2}$) T=135K, ρ=1034 kg/m^3

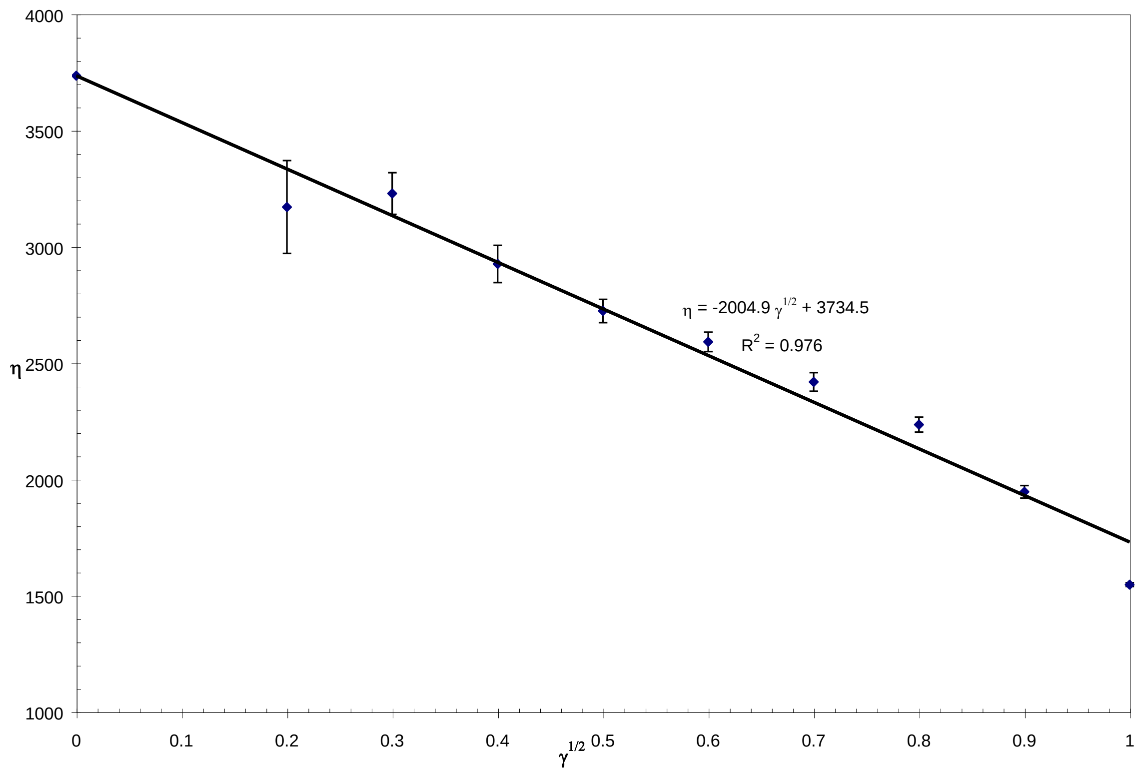

Figure 2.5: Shear viscosities (in units of 10^{-7} Ns/m^2) for krypton as a function of square root of strain rate (in units of ps$^{-1/2}$) T=135K, ρ=2315 kg/m^3

figures it is also clear that both the fluids show shear-thinning behavior since the viscosity decreases with increase in strain rate.

Shear thinning behavior is also observed in binary mixtures of argon and krypton. The extrapolations to zero strain rate of the least squares fits are used to determine the Newtonian viscosities and reported in Table 2.3. From the results we can also conclude that liquid argon and liquid krypton mixtures show non-ideality, as the viscosity values obtained from simulations are not equal to sum of the contributions from pure argon and pure krypton (the contributions weighted over the mole fractions). Further, viscosities are reported for equi-molar binary mixtures of argon and krypton for various conditions of temperature and density (Table 2.4). Good agreement was found with the available literature data.

Table 2.2: Pure argon and pure krypton systems at T=135 K. The experimental values are obtained from the literature (Heyes and Preston, 1991).

Pure Species	ρ (g/cm^3)	η(10^{-7} N s /m^2) (Experimental)	η(10^{-7} N s /m^2) (NVT MD for LJ)	%Error
Argon	1.034	740	882	19
Krypton	2.315	3016	3734	23

Table: 2.3: Simulation results for viscosity of mixtures of argon and krypton at T=135K as a function of krypton mole fraction, x. The results are compared with those available in literature (Heyes and Preston, 1991).

x	ρ(kg/m^3)	η(10^{-7} Ns/m^2) (Literature) BFW potential	η(10^{-7} Ns/m^2) (this study) LJ potential
0	1034	885	882
1/6	1267	1271	1352
1/3	1444	1502	1419
2/3	1842	2019	1511
5/6	2048	2470	1864
1	2315	3425	3734

Table 2.4: Simulation results for shear viscosity for equi-molar binary mixtures in reduced units with respect to argon LJ parameters. Comparison is made with the values available in the literature (Gardner, Heyes et al., 1991).

N	ρ^*	T^*	η^*_{lit}	$\eta^*_{this\ work}$
108	0.050	1.81	0.219	0.2231
108	0.200	1.81	0.302	0.3294
108	0.467	1.81	0.747	0.7761
108	0.818	1.81	4.006	4.7950
108	0.200	2.49	0.397	0.4750
108	0.300	2.49	0.487	0.5060
108	0.400	2.49	0.640	0.4750
108	0.500	2.49	0.860	0.8490
108	0.654	2.49	1.65	1.7400

2.4.3 Visualization of the simulations

Screen shots of a typical simulation are shown in Figures 2.6-2.8. Figure 2.6 shows the screen shot of 256 pure LJ molecules under a Couette flow. In this figure the solid lines show boundaries of the simulation box and the blue spheres represent LJ molecules. In the actual simulation we can observe the periodic boundary conditions being obeyed. Figure 2.7 shows the screen shot of velocity profile developed in the system. Velocity profile was calculated by dividing the whole simulation box into 12 bins in the y - direction and the average velocity in each bin was determined and plotted. The length of a particular arrow is proportional to the average velocity in that bin. This linear velocity profile is found to be stable for low shear rates. Figure 2.8 shows a screen shot for the velocity vectors of each particle. From the figure it is clear that particles close to the top have their velocity vectors aligned to the direction of shear because the flow represents a Couette flow with the upper plate moving in the positive x -direction.

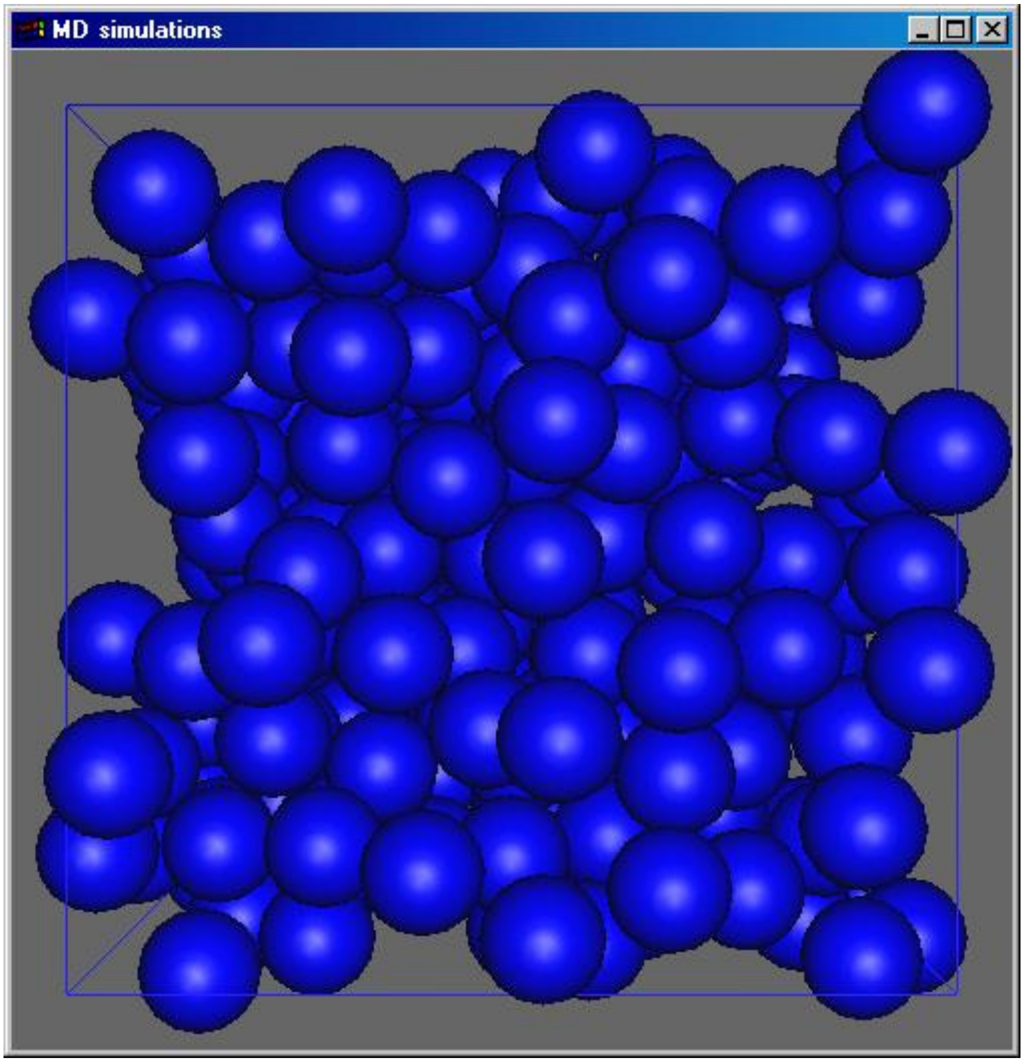

Figure 2.6: Screenshot of the simulation box showing 256 LJ molecules under Couette flow

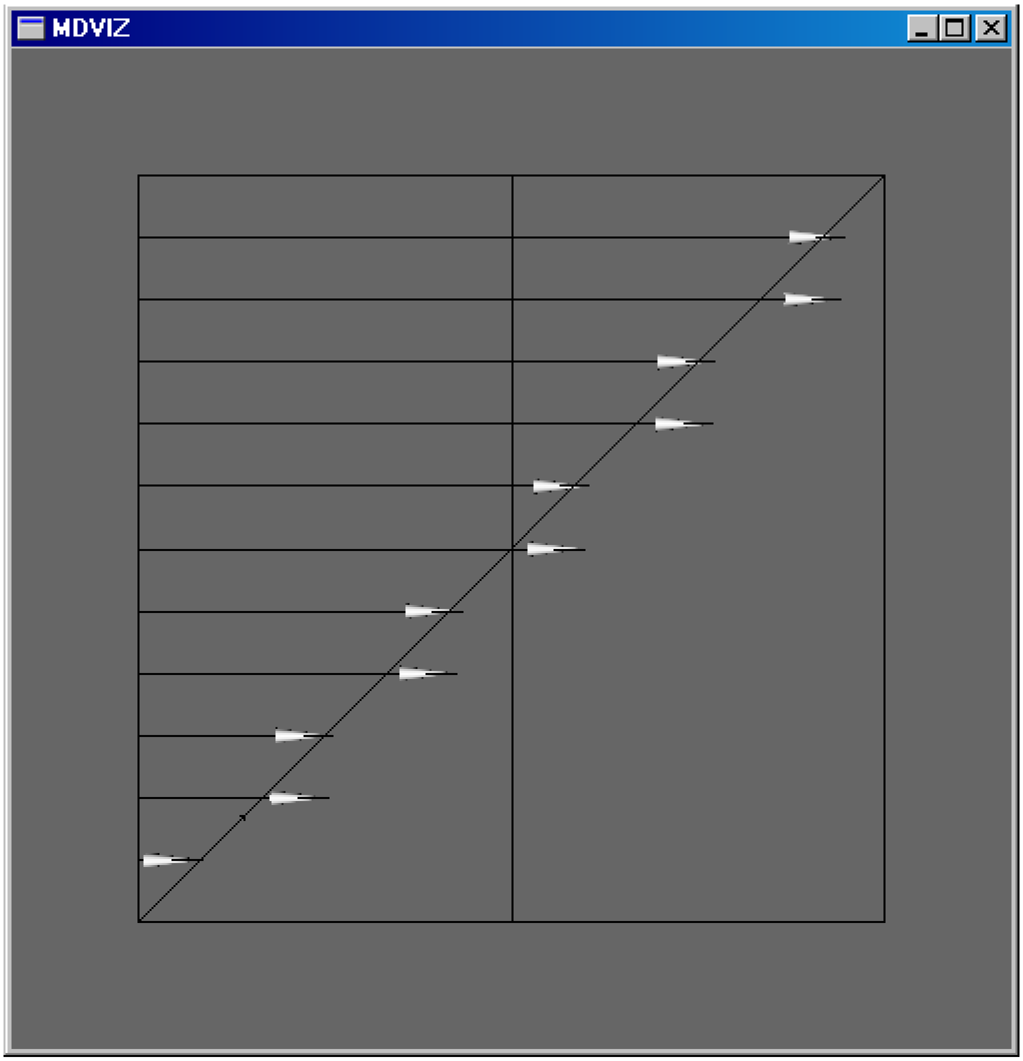

Figure 2.7: Screenshot of Couette flow velocity profile

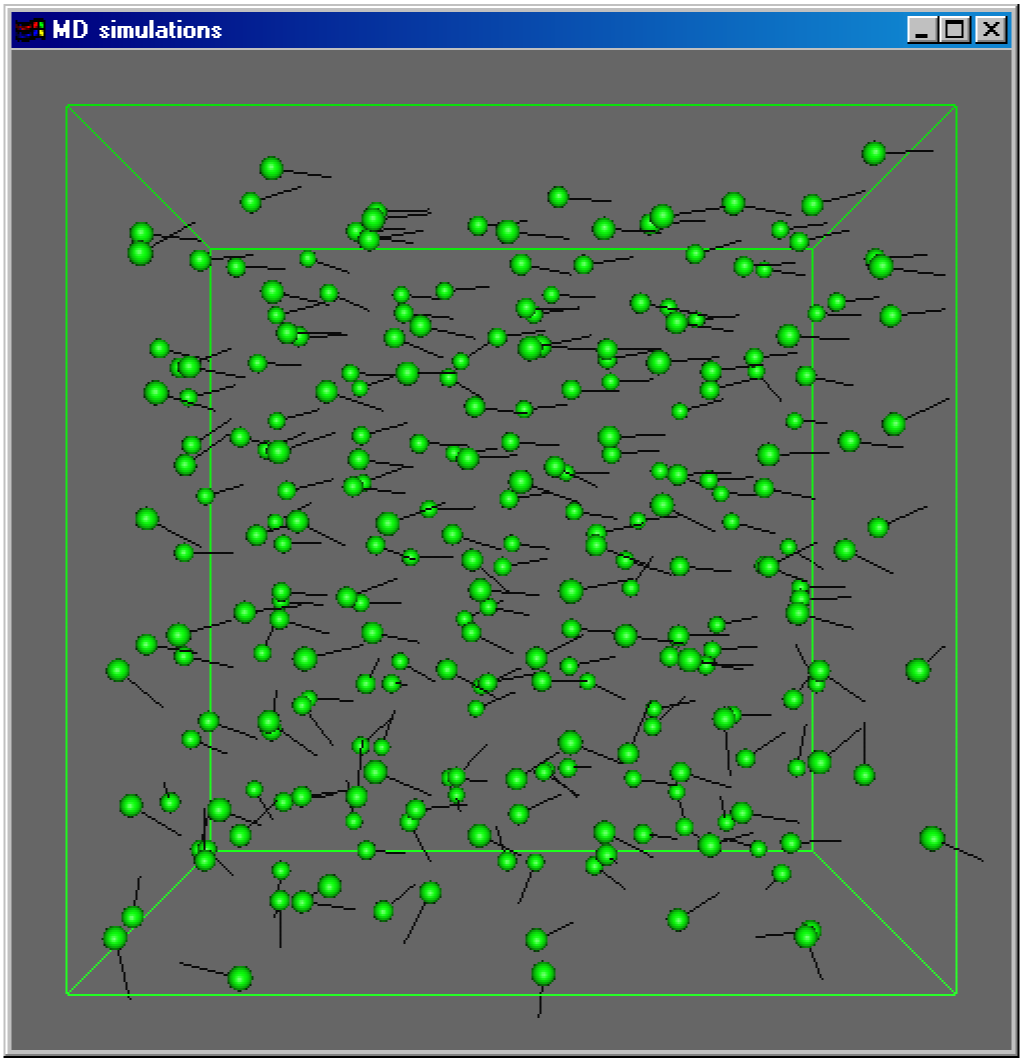

Figure 2.8: Screenshot of the simulation box showing 256 LJ molecules (subjected to Couette flow) with their velocity vectors

2.5 Simulations of structured (multiple LJ sites) molecules

Non-equilibrium MD simulations were carried out for pure carbon dioxide. Shear viscosity calculations are made for pure carbon dioxide using the methodology explained in section 2.2. Further equilibrium MD simulations were also carried out for dilute solutions of benzene in supercritical carbon dioxide with the objective of observing some special structural behavior.

2.5.1 Simulations details

As a part of this work, visualization code using OpenGL was added to the original code developed by Bansal (1996) for carbon dioxide and benzene mixtures with all units reduced with respect to the methylene site of benzene. The potential of CO_2 is the three-site linear, hetero-nuclear LJ model. Benzene is modeled as a structured planar molecule with six LJ methylene sites. The interaction parameters used in these simulations are tabulated below:

Interaction	$\sigma(A^o)$	$\varepsilon/k_B\,(K)$
C-C	2.785	29.0
O-O	3.014	83.1
CH-CH	3.35	95.05

2.5.2 Simulations results and discussion

Viscosity calculations for pure carbon dioxide were done for a density 20.091 mol/dm^3 and at a temperature T = 280 K. Viscosity versus strain rate plot is shown in Figure 2.9.

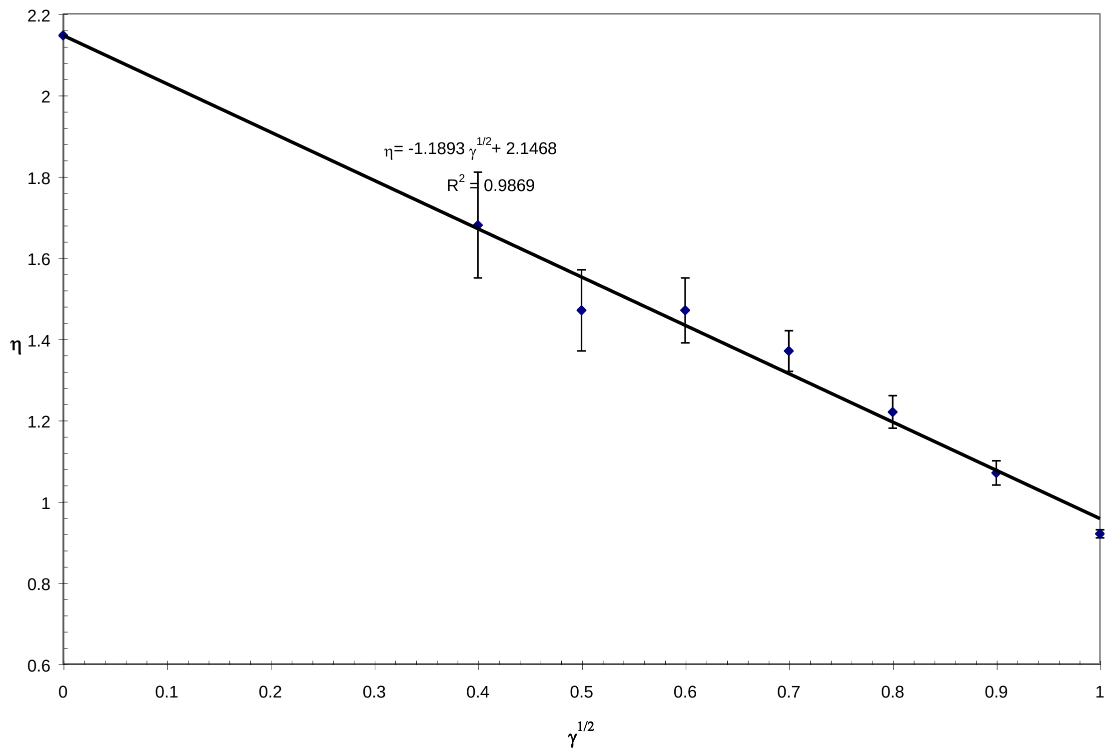

Figure 2.9: Viscosity versus square root of strain rate plot for pure carbon dioxide (in quantities reduced with respect to CH-CH site LJ parameters).

Shear thinning behavior of carbon dioxide is evident from the plot. The non-dimensional viscosity obtained from simulations is 2.15 as compared to the experimental value of 1.93. In real values they correspond to 0.1018 cp and 0.0917 cp respectively. The experimental value is obtained from the literature (Wang and Cummings, 1993).

2.5.3 Visualization of the simulations

Equilibrium MD simulations of dilute solutions of benzene in supercritical CO_2 were performed using site-site potential models for both the molecules. The simulations were carried for systems of 216 molecules (16 solute, 200 solvent) in the NVT ensemble, at slightly supercritical temperatures with respect to the solvent, and over a reduced density range of $0.5 < \rho_r < 2$. Visualization revealed that at the immediate vicinity of the benzene plane, the CO_2 molecules tend to align with their axis parallel to the benzene plane (see Figure 2.10). This behavior was earlier reported in the literature (Inomata, Saito et al., 1996). In the above-mentioned figure white spheres represent the methylene sites in benzene. The carbon dioxide molecules are represented by the combination of red and black spheres. The black spheres are the carbon sites whereas the red spheres are the oxygen sites. Throughout the simulations, it was found that structure of both benzene molecules and carbon dioxide molecules are preserved. This confirms the fact that bond length constraint equations are incorporated well in the equations of motion.

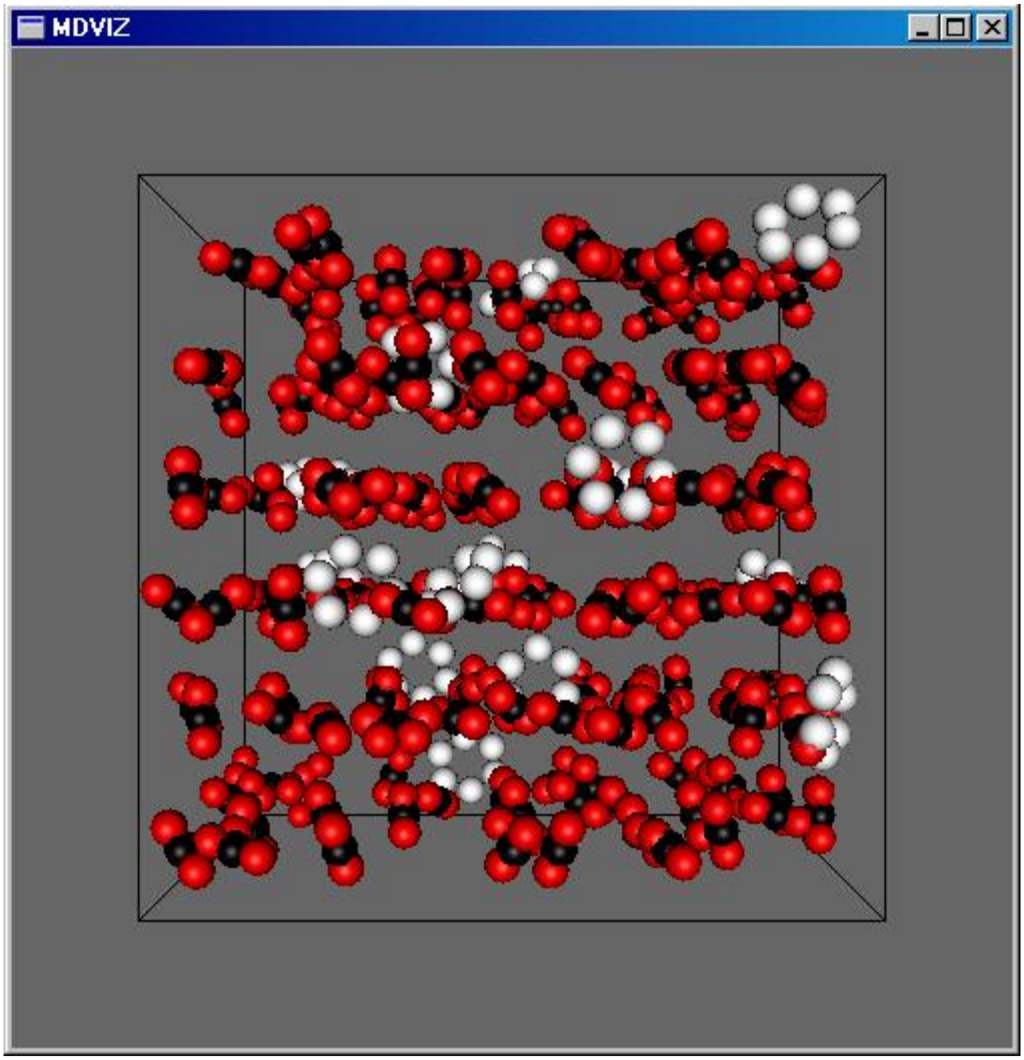

Figure 2.10: Screen shot of equilibrium simulation of dilute solution of benzene in pure carbon dioxide

D:\MyThesis\chap04.doc

Allen, M. P. and D. J. Tildesley (1989). Computer simulation of liquids. Oxford [England]
New York, Clarendon Press ;
Oxford University Press.
Evans, D. J. and G. P. Morriss (1984). "Non-Newtonian molecular dynamics." Computing phys **1**(6): 297.
Gardner, P. J., D. M. Heyes, et al. (1991). "Molecular dynamics computer simulations of binary Lennard-Jones fluid
mixtures: Thermodynamics of mixing and transport coefficients." Molecular physics **73**(1): 141.
Heyes, D. M. and S. R. Preston (1991). "Transport Coefficients of Ar-Kr Mixtures by Molecular Dynamics Computer
Simulation." Physics and chemistry of liquids **23**(3): 123.
Inomata, H., S. Saito, et al. (1996). "Molecular dynamics simulation of infinitely dilute solutions of benzene in
supercritical CO2." Fluid phase equilibria **116**(1 / 2): 282.
Lees, A. W. and S. F. Edwards (1972). J. Phys. Ser. C **5**: 1921.
Wang, B. Y. and P. T. Cummings (1993). "Non-equilibrium molecular dynamics calculation of the shear viscosity of carbon dioxide/ethane mixtures." Molecular simulation **10**(1): 1.

Chapter 3

LITERATURE SURVEY ON SUBCONTINUUM FLUID PROBLEMS

This chapter presents a literature survey on the some of the subcontinuum fluid problems that have been studied using molecular dynamics simulations. Most of these problems include fluid phenomena for which continuum fluid mechanics is inapplicable (Koplik and Banavar, 1998). Some of them are listed below:

- The rupture or coalescence of liquid drops that occur on interfacial scales is quite different from bulk continuum length or time scales. At these interfacial scales, the hydrodynamics as described by the Navier-Stokes equations breaks down (Koplik and Banavar, 1993, 1992). This particular subcontinuum fluid problem is one of the case studies in this work and dealt with great detail in the next chapter.
- Unphysical singularities that result from the application of continuum approaches, for example, corner-flow singularities (Koplik and Banavar, 1995, 1997), the Stokes drag on an object falling in a fluid as it approaches a solid surface, and the divergence of the dissipated energy when one fluid pushes another past a solid surface due to the breakdown of no-slip boundary conditions in the vicinity of moving contact lines.

- Interfacial phenomena involving thin liquid films for which the continuum approximation is not valid and the substrate-fluid interaction plays a crucial role. An example is the dynamics of spreading of wetting on solid surfaces and freezing in confined geometries (Koplik and Banavar, 2000).
- The behavior of non-Newtonian fluids for which the constitutive relationships are often unknown and the governing equations are non-linear, rendering analytic analysis difficult, if not impossible.

3.1 Corner singularities

There are a number of problems in which solutions of the Navier-Stokes equations develop an “embarrassing” divergence at “corner” points along a boundary. Examples include a sharp corner on a solid boundary (Moffat, 1964) the moving contact line when one immiscible fluid displaces another from a solid surface, and the contact point where one solid slides along another. In all such cases it was found that the solution for the shear stress varies as $T \propto r^{\alpha}$ where r is the distance from the corner point, and α depends on the problem, and may be negative. In the latter case, a divergent force of this form is not physically reasonable, and it is certainly correct to say that the continuum equations will break down at the atomic level at which point the singularity does not exist. However, further analysis is needed to provide a more definitive characterization of the flow near such points, and an MD calculation at atomic scales is an obvious candidate. Such analyses of the three examples using MD have indeed been done, and we will discuss the most recent case- flow near a "reentrant corner" where a flow suddenly contracts (Koplik and Banavar, 1997).

Consider flow in the two-dimensional channel in the Figure 3.1, where the upper and heavy lines denote solid boundaries, the system is periodic in the horizontal direction, and there is no flow variation out of the plane. The channel expands and contracts at the 270^{o} "entrant" and "reentrant" corners at the left and right, respectively, and there is no flow variation in the direction out of the plane. For a Newtonian fluid one can readily analyze the flow field near a sharp solid corner, because the no-slip boundary implies small velocities and linear Stokes equations apply. Moffat(1964) has found that $\alpha = -0.46$ at 270^{o} corner. While singular, the stress is at least square integrable and finite element and other numerical methods converge. For a non-Newtonian (NN) fluid, the constitutive relationship is both more complicated and model dependent, and there is some dispute about the value of the stress exponent, although most results give values greater than the Newtonian one. Further support from this conclusion comes from the fact that finite element calculations do not always converge. It is then appropriate to try to elucidate the behavior of NN corner flows using a molecular simulation.

Although the focus is on the reentrant corner, the entire channel is needed to generate the appropriate flow, and it is necessary to verify that the corner results are insensitive to the overall shape. Simulations have been done by earlier workers for the flow of both Newtonian and the NN fluids in a number of geometries of the form of Figure 3.1, varying both the length and depth of the upper slot, with system sizes

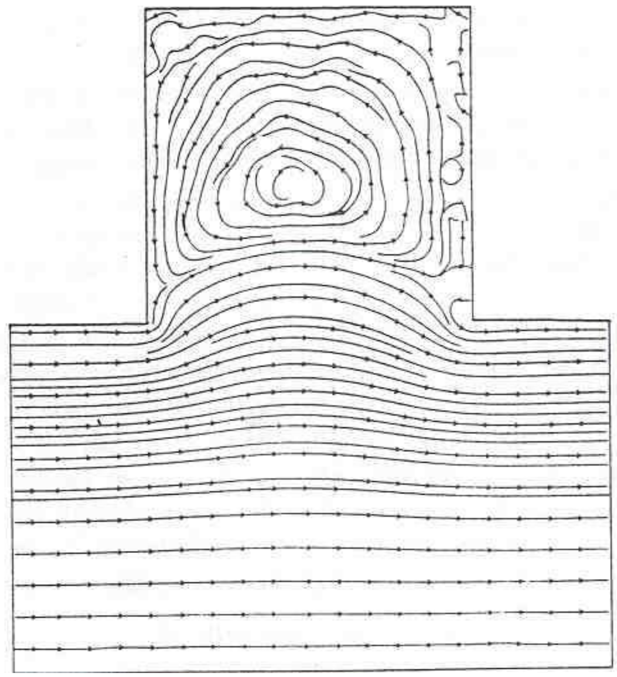

Figure 3.1: Simulation of reentrant corner flow-streamlines in an expanding/contracting channel (Koplik and Banavar, 1998)

ranging from about 13,000 to 122,000 atoms (Koplik and Banavar, 1997. For all the Newtonian flows, the Moffat value of the stress exponent, was reproduced to an accuracy of ±5%. For the NN fluids Koplik and Banvar (1997) report that the it appears to saturate at a value of –0.8 and also they observed a clear enhancement of the molecules in the regions of high stress at the corners and near the main channel walls.

3.2 Short distance lubrication

This involves study of fluid flow around a sphere immersed in a viscous liquid moving towards a wall at constant velocity. The drag force on the sphere is modified from the Stokes value because fluid must be expelled from the gap between the sphere and the wall and furthermore, in such lubrication problems, one expects a divergence, as the gap size tends to zero. The continuum calculations of Brenner (1961) give a limiting force:

$$F = 6\pi\mu Ub\left(\frac{b}{h}+\cdots\right) \tag{3.1}$$

where the sphere has radius b and velocity U, the gap size is h and the fluid viscosity is μ. These results were tested by an MD simulation in which relatively small spheres of radius 3 in reduced units, with and without an internal molecular structure, were moved towards a wall at a speed of $U = 2$ in reduced units. Here a structured ball is a spherical region of FCC lattice, while "without structure" means a single Lennard-Jones atom of that radius. A typical result is shown in Figure 3.2, which gives force *vs* gap size. The

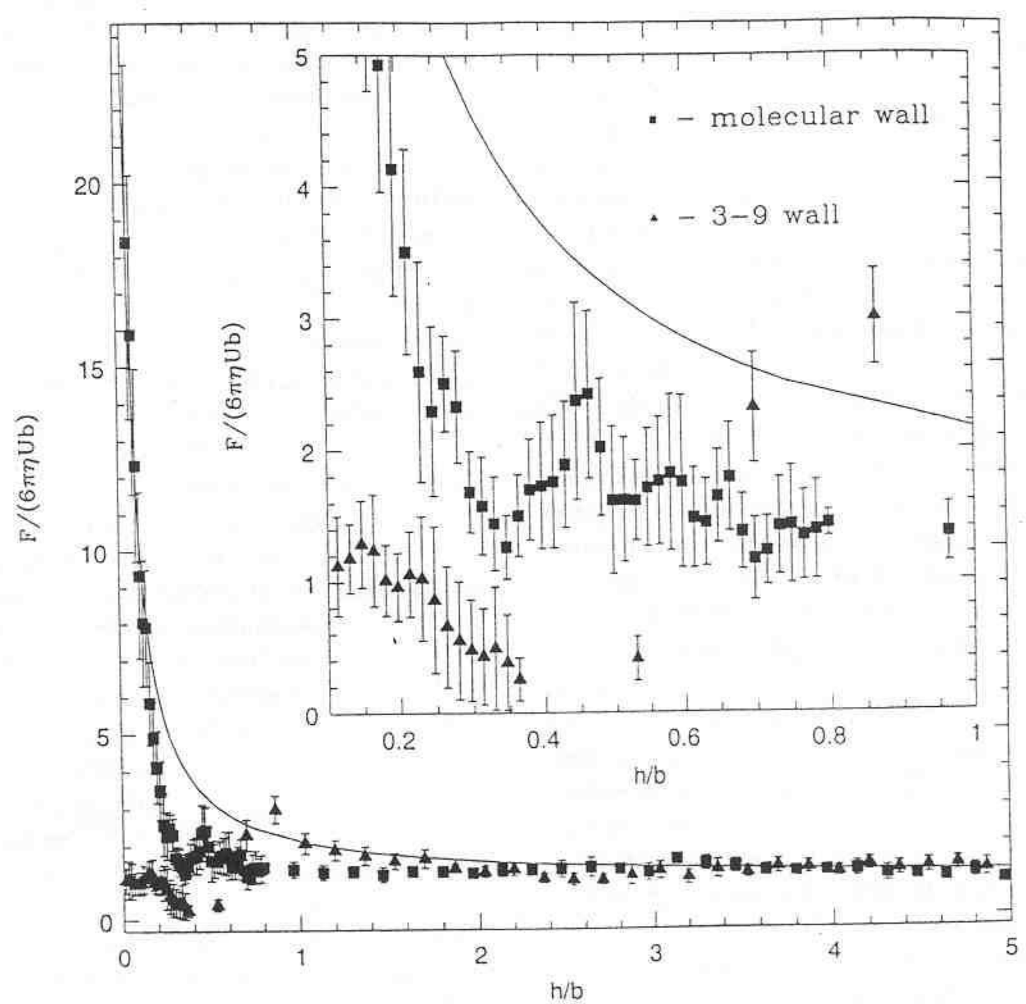

Figure 3.2: Force on a sphere approaching a solid wall (Koplik and Banavar, 1998)

general conclusion to be drawn Figure 3.2 is that as long as the gap size is larger than 2-3 fluid molecule diameters, the continuum and MD forces agree well. In particular, in the limit of large separation the free fluid Stokes drag formula is reproduced within the statistical errors. For small separation, there is a discrepancy: the MD force does not diverge. And in fact, drops back to small values for very small gaps. The origin of the latter behavior is simply that eventually all of the fluid molecules are squeezed out of the gap and there is no longer any lubrication layer.

Chapter 4

COALESCENCE AT LIQUID–LIQUID INTERFACE

In the first few sections of this chapter, the coalescence phenomenon and the hydrodynamic models that explain experimental observations are discussed. The need for MD simulation studies of coalescence process is then discussed. The last section presents results of simulations carried out as a part of this work.

The problem of coalescence is fundamental to the study of heterogeneous systems. When mass is transferred between two fluids, it is usual to disperse one fluid in the other in the form of drops or bubbles. This occurs in both differential contactors and stage-wise contactors. When mass transfer is complete, the drops must be recombined to reform the bulk phase before it can be processed further. The drops may coalesce with each other, but finally coalescence at the bulk interface must take place. Problems often occur because the rate of coalescence is too slow, or because a secondary haze is formed which contaminates the continuous phase. In order to overcome such difficulties it becomes important to understand the basic mechanism governing coalescence. Some of the other applications where study of coalescence is important are (a) preparation of stable emulsions, foams and dispersions (b) formation of a bank during displacement of oil from reservoir rock (c) and displacement of unstable foam used for mobility control in a tertiary oil recovery process.

Coalescence at a liquid-liquid interface can be of two types (a) coalescence of two drops of liquid into a single drop (b) coalescence of a drop of a liquid with its mother phase at a liquid-liquid interface. In this chapter we focus on the latter type.

4.1 Coalescence Phenomenon

The mechanism of drop coalescence was observed to occur in the following successive steps as shown in Figure 4.1.

1. The drop (phase 1) approaches the interface, is decelerated, and may oscillate moderately. Both the drop and interface deform.
2. The drop and interface enclose a thin layer of continuous phase (phase 2), which has to drain to a critical low thickness. During the drainage, the drop apparently rests on the interface.
3. Finally, the layer (phase 2) ruptures and drop can flow into its mother phase (phase 1). This flow-in process is often not completed and a secondary drop remains. This is termed as “partial coalescence”.

Based on these observations, “drop rest-time” or “coalescence time” is defined in the following manner: when a drop of liquid (phase 1) falls gently through a lighter, immiscible liquid (phase 2) onto a flat interface separating two phases, it rests on latter for a time t_c before coalescing with the underlying phase. This time is termed as

Approach of a drop (phase1) to horizontal liquid-liquid interface

Film drainage of thin layer of continuous phase (phase 2).

Rupture of thin layer.

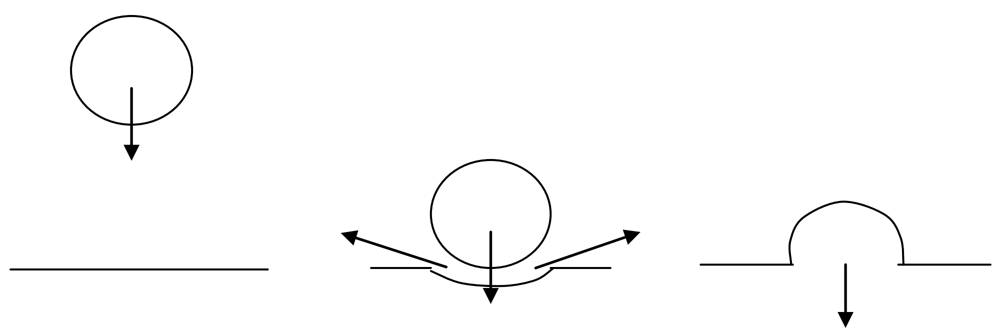

Figure 4.1: Course of coalescence process of a single droplet at plain liquid-liquid interface (Rommel, Menon et al., 1992).

drop rest time. Coalescence time characterizes any coalescence process. Considerable research was done in determining the coalescence time for various systems. Some of the studies on coalescence times reported that the coalescence times of drops are not constant, but vary under the experimental conditions. While studying sufficient numbers of drops of the same size one at a time, Charles and Mason (1960) reported a distribution of coalescence times. A typical plot, of integral distribution function *f* of drop rest-times of water drops coalescing at a toulene/water interface at 20^{o}C is shown in the Figure 4.2. Curves 1 to 4 represent drop diameters of 0.384, 0.544 and 0.604 cm respectively. The complex interactions of various influencing effects make the coalescence seem to be a stochastic process. Here is the list of some of those influencing factors reported by earlier workers:

- Nature of the fluids
- Drop diameter
- Age of the interface
- Presence of surface-active agents at the interface
- Temperature and shear gradients
- Mass transfer between phases
- Temperature of the system
- Presence of thermal, sonic, mechanical and other disturbances

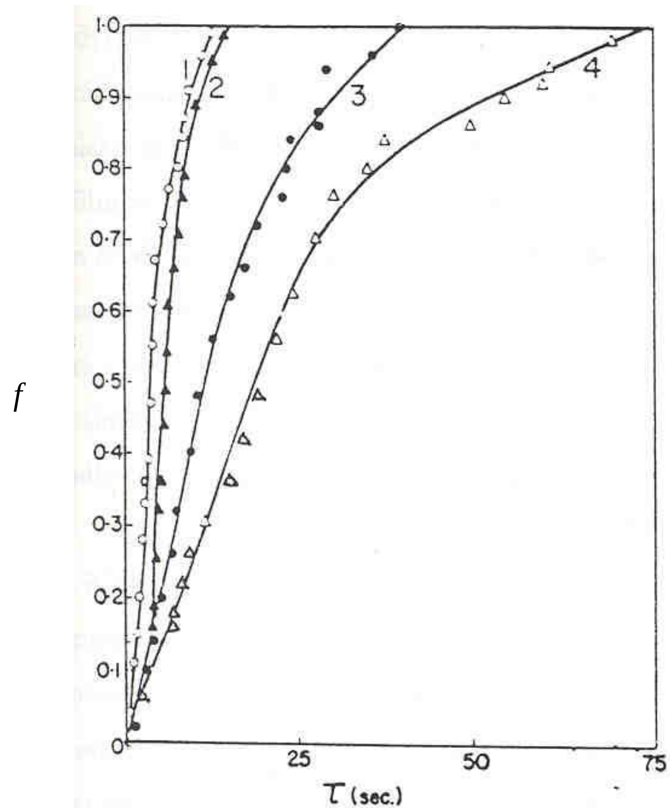

Figure 4.2: Integrated drop rest time distribution curve (Charles and Mason, 1960)

Charles and Mason (1960) worked with various systems like water-benzene, carbon tetra chloride-water. They found that:

1. t_c (drop rest time) shows a roughly Gaussian distribution between $t_{\min}$ and $t_{\max}$.
2. Drop stability increases with decreasing temperature and with increasing drop size.
3. With oil-water system, t_c was markedly reduced when the drop contained small amounts of a diffusing component, when an electrostatic field was applied or when the interface was contaminated with solid particles.

Hodgson and Woods (1969) worked with systems like water-toulene, water-anisole and surfactants like sodium lauryl sulfate. Their work confirmed the effect of interface age and drop diameter on drop rest times. Lang and Wilke (1971) observed that the average t_c is less for systems having smaller interfacial tension. Their studies revealed that t_c decreased when sonic disturbances were introduced. Also, their observations strongly supported the fact that presence of surfactants increase the drop rest times. Aderangi and Wasan (1995) made investigations with droplets of ethyl benzene at the interface of homophase, water. They found that the droplets were indefinitely stabilized by polyvinyl alcohol, a non-ionic surfactant.

4.2 Models of coalescence

Most coalescence models either calculate the time for drainage of a thin layer between the approaching drop and interface or the approaching velocity between them. In calculating the drop rest time, it is assumed that once the film thickness is reduced to less than critical thickness h_{cr}, the rupture process takes over, and the coalescence is rapid so that one can neglect the rupture time. The values of critical thickness are calculated by substituting time of coalescence obtained experimentally in t_c relations given by various models. Vrij and Overbeek (1968) gave a relation to calculate the critical thickness.

$$h_{cr} = 0.267\left[\frac{a_f A_m^{\ 2}}{6\pi\sigma\Delta p}\right]^{\frac{1}{7}} \tag{4.1}$$

where A_m is the Hamaker constant, Δp is the excess pressure in the film, σ is surface tension and a_f is the film area. In most of the experiments the value of h_{cr} is always less than 5A^o (diameter of argon atom is 3.45 A^o). This thickness corresponds to nearly one or two molecular layers. At this film thickness, London van der Waals forces and double layer forces are significant. One of the coalescence models is discussed here.

4.3 Parallel disc model

It is one of the earliest models of coalescence proposed by Charles and Mason (1960). The model is based on two parallel and circle-shaped discs with rigid surfaces separated by thin film, which approach each other (see Figure 4.3). The discs correspond to the contact area of the drop with the interface. The various steps involved in the process of coalescence: (a) drop deformation (b) film thinning and (c) film rupture and collapse are modeled in the manner described below.

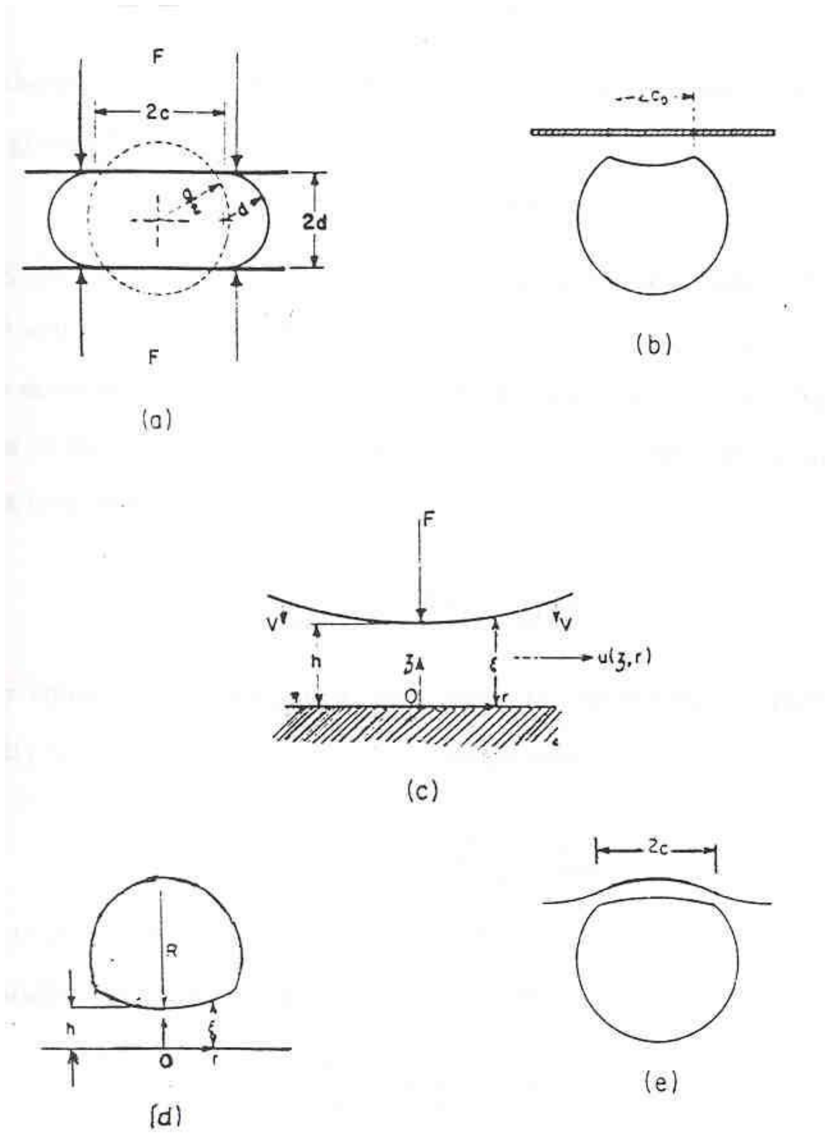

Figure 4.3:(a) Deformation of a drop contained between two parallel planes. (b) Bubble profile at the rigid flat surface. (c) The close approach of surfaces immersed in a viscous fluid. (d) Idealized drop profile at rupture. (e) Proposed profile at the interface (Charles and Mason, 1960).

4.3.1 Drop deformation

The deformation of a drop under the compressive force is estimated by considering it to be contained in a fluid between two parallel planes, which are pushed together with a force F until equilibrium is reached. Let a be the diameter of undistorted spherical drop and $2d$ the equilibrium separation between the two planes. For simplicity, it is assumed that the bulging interface between the planes has a semicircular profile of radius d and the drop interface adjacent to the plane is a flat disc of radius c. At equilibrium force F is balanced by Δp (excess pressure) inside the drop**.**

$$\begin{aligned} F &= \Delta p \pi c^2 \\ \Delta p &= \sigma\left[\frac{1}{d} + \frac{1}{d+c}\right] \end{aligned} \tag{4.2}$$

From volume conservation (drop fluid assumed to be incompressible) and assuming the distortion is very small, $d = b$ and after simplification we get

$$c = \frac{4}{\pi}(b-d) \tag{4.3}$$

$$F = \frac{2\pi\sigma}{b}c^2 \tag{4.4}$$

For the case of a drop resting on a plane surface and deformed by its own weight, Eqn (4.4) reduces to

$$c = b^2\left[\frac{2\Delta\rho g}{3\sigma}\right]^{\frac{1}{2}} \tag{4.5}$$

where $\Delta\rho$ is the difference in the density of the drop and surrounding medium and g is the acceleration due gravity.

4.3.2 Film thinning

A simple new equation for rate of film thinning is derived by use of number of simplifying assumptions for a film of generalized profile. Consider a rigid surface immersed in a viscous fluid and rotationally symmetrical about the z-axis, to approach a flat stationary plane from above in response to a constant force F as illustrated in Figure 4.3. Let the minimum separation at any time t be given by $z = h$ at $r = 0$, where z and r are measured from the origin located in the stationary plane. Let $V = -dh/dt$ be the velocity of the approaching surface at any time t. During the approach, the incompressible fluid having viscosity η_2 is expelled radially from between the surface at a velocity $u(z,r)$. It is assumed that the flow is laminar, radial (i.e., the z component of fluid velocity is zero) and the inertial effects are negligible. At a distance r from the origin, let the separation be ξ and assume the radial velocity $u(z,r)$ to be given by

$$u(z,r) = z(\xi - z)\psi(r) \tag{4.6}$$

where $\psi(r)$ is a function of r. Since the surfaces are assumed to be rigid, $u(z,r) = 0$ at $z = (0,\xi)$. This is the "no slip" boundary condition.

By considering the flux at $(r + dr)$ of the draining fluid and equating the change in flux to the volume of liquid displaced by the approaching surface in unit time between r and $(r + dr)$, we obtain

$$u(z,r) = \frac{3z(\xi - z)Vr}{\xi^3} \tag{4.7}$$

and by equating the mechanical work done to the energy dissipated due to viscosity the following relationship is obtained

$$V = -\frac{dh}{dt} = \frac{F}{6\pi\eta_2 \int_0^r \frac{r^3}{\xi^3} dr} \tag{4.8}$$

where η_2 is the viscosity of the draining fluid.

For a parallel disc approach $\xi = const = h$ gives

$$\frac{dh}{dt} = -\frac{2F}{3\pi\eta_2 c^4} h^3 \tag{4.9}$$

On integrating the above equation from $h = h_1$ to $h = h_2$ and assuming that a liquid drop of radius b approaches a flat interface under its own weight and deforms, we obtain on substituting for F and c, the expression for coalescence time.

$$t_c = \frac{\eta_2}{4} \left[\frac{\Delta\rho g b^5}{\sigma^2} \right] \frac{1}{h_2{}^2} \tag{4.10}$$

where it is assumed that $h_1 >> h_2$.

4.3.3 Film rupture and collapse

Following the formation of a hole in the phase 2 film, the interfacial tension will act to reduce the interfacial area. Assuming that the surface free energy released is completely converted into kinetic energy of the liquid displaced from the hole, an equation was also derived for the velocity of hole expansion.

It must be emphasized that the following model assumes that interfaces are rigid and thus resists shear stresses due to finite velocity gradient on each surface. It is also subject to several limitations namely negligible electro viscous effects and London-van der Waals force of attraction. Rigid behavior however was reported to occur with low velocity gradients, high interfacial tension, small bubble diameters and in the presence of surfactants. This model could explain only the effect of hydrodynamic parameters on t_c, but could not explain drop rest time distribution, the effect of interface age, and presence of surface-active agents. The expression developed for coalescence time in this model overestimates the experimental values. However, this model had been the fundamental basis for all the subsequent deterministic models. But no single model to date could explain satisfactorily all the findings.

Recently some models had also been proposed to explain the stochastic behavior of the drop rest time distribution. Jeelani and Hartland (1994) tried to give an explanation for this stochastic behavior. According to them disturbances cause rupture of the film and facilitates coalescence. It was assumed that a disturbance having an angular frequency, q generates a sinusoidal wave of wavelength, λ, and wave number, $k = 2\pi\lambda$, in the interface between the bulk phase-1 and phase-2 fluids. This wave is propagated into the lower interface of the phase-2 film. A wave will also be formed in the upper interface of the phase-2 film. If the amplitudes of either or both waves become equal to the film thickness in any region, the film will be ruptured, creating a hole through which the drop material can flow into the bulk (phase 1) material causing drop coalescence.

Two types of film rupture were considered by Lang and Wilke (1971). The first type is due to Taylor instability and the second type considers the effect of large disturbances of a film. The Taylor instability describes the mechanism by which an infinitesimal disturbance of proper wavelength can grow to amplitude large enough to rupture the film. However, Taylor instability is restricted to a definite wave number range. i.e., not all waves/disturbances are capable of causing rupture. A very intense disturbance having any wave number can generate waves sufficiently large in amplitude to directly rupture the film, even though its wavelength is too short to promote an unstable situation. This film rupture model accounts for the fact that the film disintegrates in much less time than that calculated from the drop-approach model alone. The general shape of the distribution curve is due to the random arrival of disturbances.

4.4 MD simulation of coalescence process

The coalescence process is on the whole a problem of continuum fluid mechanics. But the fine structure of the rupture and the recombination of the drops at interfacial boundaries occur at molecular scales. Coalescence modeling based on the Navier-Stokes equation successfully captures the evolution of drop shape but lacks the boundary condition or rule derivable from the first principles for sewing two interfaces together. The rupturing of the thin film is very poorly understood and cannot be modeled by using hydrodynamic equations. In order to get an insight into the rupture process, one can perform MD simulations since the rupture process takes place at length scales comparable molecular diameters.

As a part of this study, MD simulations were performed to observe the coalescence phenomena. The system that was simulated is an immiscible mixture of two liquids: one representing a heavier phase and the other representing the lighter phase. A drop of heavier phase is introduced into the lighter phase at a small distance (two molecular layers) from the interface. The system is then observed as the drop coalesces with its mother phase (heavier phase).

4.4.1 Simulation details

The simulations were carried on a total of 864 LJ molecules at reduced temperature T=0.8 and a density ρ=0.8. At these conditions the system represents a liquid on the LJ phase diagram.

The simulations were started with the molecules in a face centered cubic lattice (Figure 4.4). The blue spheres represent the heavier phase and the green spheres represent the lighter phase. The interface is formed approximately at the center of the simulation box. The upper half of simulation box is filled completely with one species and represents the lighter phase. The bottom half is filled with the other species and represents the heavier phase. The composition is approximately 50% heavier phase and 50% lighter phase. However the same σ and ε are used for all the molecules. The system is equilibrated for a time interval of 15,000 steps and then a drop (it is modeled as cylinder with its axis parallel to the interface) consisting of a few molecules of heavier phase is introduced in the lighter phase. This drop is introduced very close to the interface (two molecular layers apart). On all the molecules of the drop, a force in the negative y

direction and of magnitude $g = 0.3\sigma / \tau^2$ (in reduced units) is added. This force is responsible for the coalescence to occur. If we compare to experiments, this force represents the gravitational force due to difference in densities of the two liquid phases.

In all the simulations, molecules were allowed to interact by the familiar Lennard-Jones potential

$$V_{ij}(r) = 4\varepsilon[c_{ij}(r/\sigma)^{-12} - d_{ij}(r/\sigma)^{-6}] \tag{4.11}$$

where i and j refer to the molecular pairs in the system. For a simulation involving a single species, one normally chooses $c = d = 1$. But in this case, we have two species. The immiscibility of the two liquids was forced by setting $d_{12} = 0$ and $d_{11} = d_{22} = 1$. In all the cases, $c_{ij} = 1$.

Regular periodic boundary conditions were applied both in x and z directions, but in the y direction, the walls were modeled as solid walls. This was achieved by assigning very high masses to the layers of molecules close to the y boundaries (say $m = 100000$ in reduced units). This ensures that the above-mentioned layers of molecules remain stationary and behave as solid walls.

4.4.2 Simulation results and discussion

The visualization of simulations revealed that the system indeed equilibrated after 15,000 steps and the interface was found to be stable. After 15,000 steps, a liquid drop of heavier phase (blue spheres) consisting of 30-40 molecules was introduced two molecular layers above the interface. The geometry of the drop fluctuates as the constituent molecules and try to find a hole in the molecular layer separating them from its bulk phase. After another 10,000 steps, a sufficiently big hole was found and the entire drop slowly gets sucked in to the bulk phase by the mutual attractive force between the bulk phase and drop molecules. Most of the molecules of the drop merged with the bulk phase. Then the hole was zippered by the molecules of other species. The entire merging process took around 30,000 time steps. But there were some drop molecules left out. This behavior (also termed as partial coalescence) was also reported in the literature experimental data. Screen shots of the various stages of coalescence are shown in Figure 4.4.

Although the simulations seemed to have mimicked the coalescence process, it was difficult to extract a boundary condition (which Navier-Stokes equations could also not provide) for the rupturing of the interface and quantify the calculations. The system size (864 molecules) is too small to actually study the velocity fields and stress fields near the interface when the rupture of film occurs. Perhaps a system size close to 20,000 molecules and drop size of 2000 molecules will give a better picture of the velocity and stress fields.

In these simulations, the rupture process seemed to have occurred due to the thermal fluctuations. Based on the experiment results, it is believed that there are many influencing factors for coalescence to occur. In experiments, it is not possible to isolate the influence of each of these factors, whereas we enjoy more freedom while performing simulations. Although not studied in this work, one could actually study the effect of surfactants, effect of temperature or shear gradients on the coalescence process using simulations.

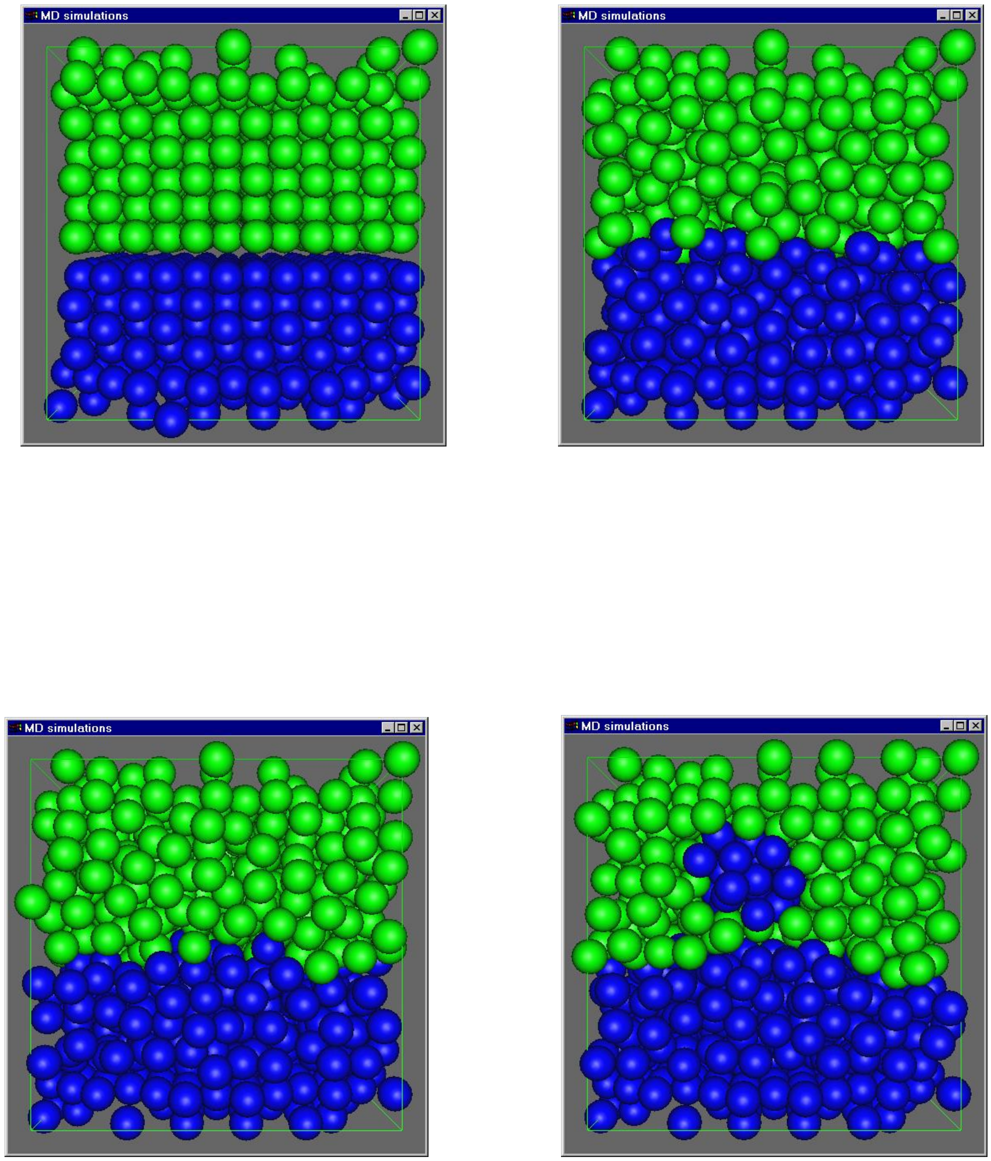

Figure 4.4 (a): Screen shots of coalescence process at time steps N=50, 10000, 12000, and 15000 respectively.

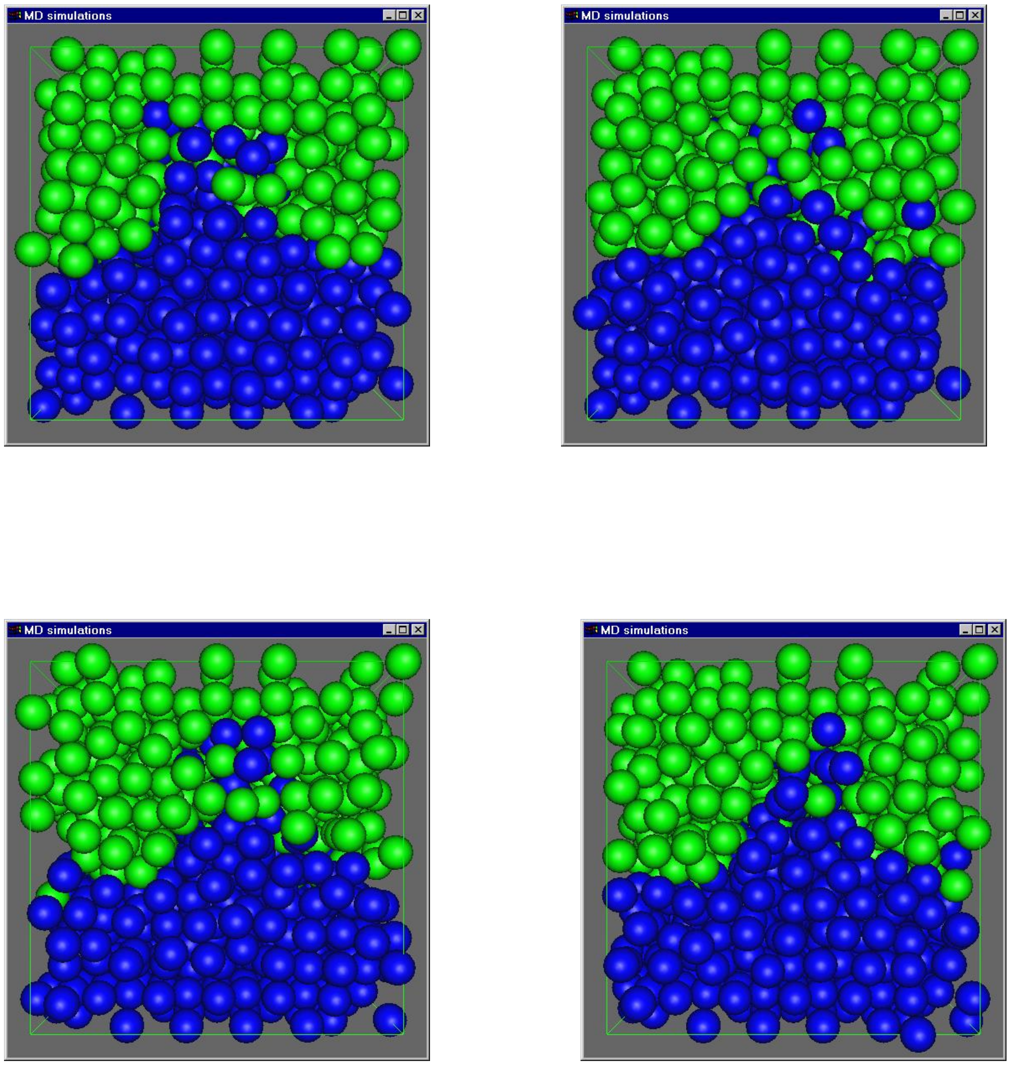

Figure 4.4 (b): Screen shots of coalescence process at time steps N=20000, 25000, 30000, and 35000 respectively.

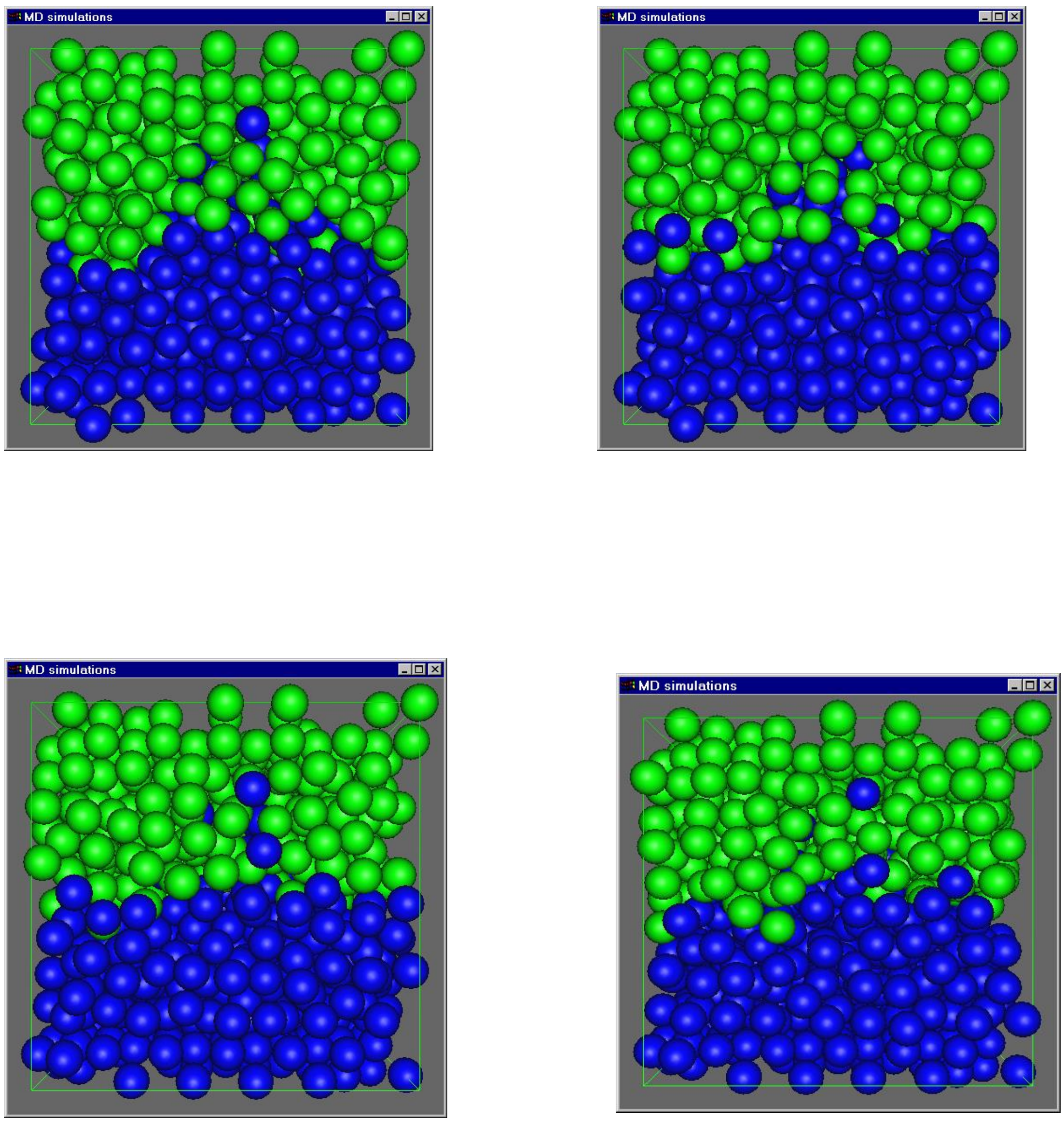

Figure 4.4 (c): Screen shots of coalescence process at time steps N=40000, 45000, 50000, and 55000 respectively.

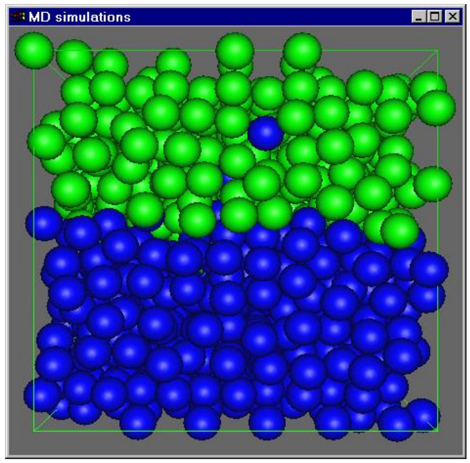

Figure 4.4 (d): Screen shot of coalescence process at time steps N=80000

Chapter 5

CONCLUSIONS AND RECOMMENDATIONS

In this work, computer programs (available in the accompanying CD) were developed for the molecular level simulation of various Lennard-Jones fluid systems. Using these programs, a series of non-equilibrium molecular dynamics simulations were performed to determine the shear viscosity of pure liquid argon, pure liquid krypton, binary liquid mixtures of argon and krypton at varied compositions. The simulation results were examined using real time visualization. The above-mentioned computer programs with some modifications were then used to study one of the subcontinuum fluid problems: coalescence of liquid drops at liquid-liquid interface. In addition, visualization code was added to a computer program developed by Bansal (1996) for MD simulations of benzene-carbon dioxide mixtures. Following are the findings of this study:

1. Shear viscosity calculations based on LJ potential model overestimated the experimental values of argon and krypton by 19% and 23% respectively.

2. Shear viscosity results for binary mixtures of liquid argon and liquid krypton revealed that both argon and krypton form non-ideal mixtures. The results obtained were found to match well with the literature data.
3. Shear viscosity of pure carbon dioxide at a density of 20.091 mol/dm^3 and at temperature 280 K was obtained within 10% of the experimental value.
4. Shear thinning is evident for all the fluids and fluid mixtures examined in this study.
5. Visualization proved to be a strong validation tool for MD viscosity calculations. It provided a better way to monitor the system as it evolves and observe any kind of special behavior it exhibits.
6. Visualization showed various steps involved in the coalescence process. It gave better insight of the process but the objective of obtaining a boundary condition for the rupture step of the coalescence process was not fulfilled.

Based on this study, I propose the following areas for future work:

1. Structured molecules under shear were reported to show changes in structure or conformations. Visualization of their simulations can reveal this interesting behavior.
2. One can study the coalescence process with larger system size and see if one can come with a boundary condition for rupture step by analyzing the velocity and stress fields near the interface during rupture process. Also, it will be of interest to study the effect of temperature and shear gradients and the presence of surface-active agents on the coalescence process.

NOMENCLATURE

a	Diameter of undistorted spherical drop, m
a_f	Area of film, m^2
A	Dynamical quantity
A_m	Hamaker constant, Nm
$\mathbf{c}$	Peculiar or thermal velocity, m/s
E	Total energy, J
E_k	Kinetic energy, J
$\boldsymbol{F}_{ij}$	Intermolecular force between atoms i and j, N
g	Acceleration due to gravity, ms^{-2}
h_c	Critical film thickness, m
H	Hamiltonian, J
k_B	Boltzmann's constant
K	Kinetic energy, J
L	Simulation box length, m
m	Mass, kg
N	Number of particles
Δp	Excess pressure inside the drop, N/m^2

$\mathbf{p}$	Momentum vector of a particle, kg m/s^2
P	Pressure, N/m^2
$\mathbf{r}_i$	Cartesian coordinate of i^{th} particle, m
t	Time, s
T	Temperature, K
$\boldsymbol{u}$	Streaming velocity, m/s
U	Configurational energy, J
V	Volume, m^3
ε	Characteristic energy in pair potential, J
η	Shear viscosity, Ns/m^2
ρ	Number density, particles/m^3
σ	Characteristic distance in pair potential, m
$\boldsymbol{\tau}$	Shear stress tensor, N/m^2
γ	Strain rate, s^{-1}
$\langle \cdots \rangle$	Ensemble average
*	Superscript used for representing non-dimensional units

REFERENCES CITED

Aderangi, N. and D. T. Wasan (1995). "Coalescence of single drops at a liquid-liquid interface in the presence of surfactants/polymers." Chemical engineering communications **132**: 207.

Allen, M. P. and D. J. Tildesley (1989). Computer simulation of liquids, Oxford science publications.

Bansal, V. (1996). "Molecular dynamics studies of rheology in fluid mixtures." PhD. dissertation, Dept. of chemical engg. Golden, Colorado school of Mines**:** 261.

Brenner, H. (1961). Chemical engineering science **16**: 242.

Charles, G. E. and S. G. Mason (1960). "The coalescence of liquid drops with liquid/liquid interfaces." Journal of colloid science **15**: 236.

Edberg, R., G. P. Morriss, et al. (1986). "Constrained molecular dynamics: simulations of liquid alkanes with a new algorithm." Journal of chemical physics **84**: 6933.

Evans, D. J. and G. P. Morriss (1984). "Non-Newtonian molecular dynamics." Computing phys **1**(6): 297.

Gardner, P. J., D. M. Heyes, et al. (1991). "Molecular dynamics computer simulations of binary Lennard-Jones fluid mixtures: Thermodynamics of mixing and transport coefficients." Molecular physics **73**(1): 141.

Haile, J. M. (1997). Molecular dynamics simulation : elementary methods. New York, Wiley.

Hartland, S. (1967). "The coalescence of liquid drop at a liquid-liquid interface." Transactions of the institution of chemical engineers **45**: 97.

Heyes, D. M. and S. R. Preston (1991). "Transport coefficients of Ar-Kr mixtures by molecular dynamics computer simulation." Physics and chemistry of liquids **23**(3): 123.

Hodgson, T. D. and Woods. (1969). "The effect of surfactants on the coalescence of a drop at an interface." Journal of colloid science **30**: 429.

Inomata, H., S. Saito, et al. (1996). "Molecular dynamics simulation of infinitely dilute solutions of benzene in supercritical CO2." Fluid phase equilibria **116**(1 / 2): 282.

Koplik, J. and J. R. Banavar (1992). "Molecular structure of the coalescence of liquid interfaces." Science **257**: 1664.

Koplik, J. and J. R. Banavar (1993). "Molecular dynamics of interface rupture." Physics of fluids **5**(3): 521.

Koplik, J. and J. R. Banavar (1995). "Corner flow in the sliding plate problem." Physics of fluids **7**(12): 3118.

Koplik, J. and J. R. Banavar (1997). "Molecular simulation of Reentrant corner flow." Physical review letters **78**(11): 2116.

Koplik, J. and J. R. Banavar (1998). "Molecular simulation of viscous flow." JSME International Journal **41**(2): 353.

Koplik, J. and J. R. Banavar (1998). "Physics of Fluids at Low Reynolds Numbers--A Molecular Approach." Computers in physics **12**(5): 424.

Koplik, J. and J. R. Banavar (2000). "Molecular simulations of dewetting." Physical review letters **84**(19): 4401.

Lang, S. B. and C. R. Wilke (1971). "A hydrodynamic mechanism for the coalescence of liquid droplets." Industrial and engineering chemistry fundamentals **3**: 329.

Lees, A. W. and S. F. Edwards (1972). Journal of physics section C **5**: 1921.

Moffat, H. K. (1964). Journal of fluid mechanics **18**: 1.

Neider, J., T. Davis, et al. (1999). OpenGL programming guide : the official guide to learning OpenGL. Reading, Mass., Addison-Wesley.

Rapaport, D. C. (1995). The art of molecular dynamics simulation. Cambridge ; New York, Cambridge University Press.

Rapaport, D. C. (1997). "Interactive molecular dynamics." Physica a : statistical and theoretical physics **240**(1 / 2): 246.

Rommel, W., W. Menon, et al. (1992). "Hydrodynamic modeling of droplet coalescence at liquid/liquid interface." Separation science and technology **27**(2): 129.

Vergeles, M., P. Keblinski, et al. (1995). "Stokes drag at the molecular level." Physical review letters **75**(2): 232.

Vrij, A. and J. T. G. Overbeek (1968). "Rupture of thin liquid films due to spontaneous fluctuations in thickness." Journal of American chemical society. **90**: 3074.

Wang, B. Y. and P. T. Cummings (1993). "Non-equilibrium molecular dynamics calculation of the shear viscosity of carbon dioxide/ethane mixtures." Molecular simulation **10**(1): 1.